CHALMERS
UNIVERSITY OF TECHNOLOGY

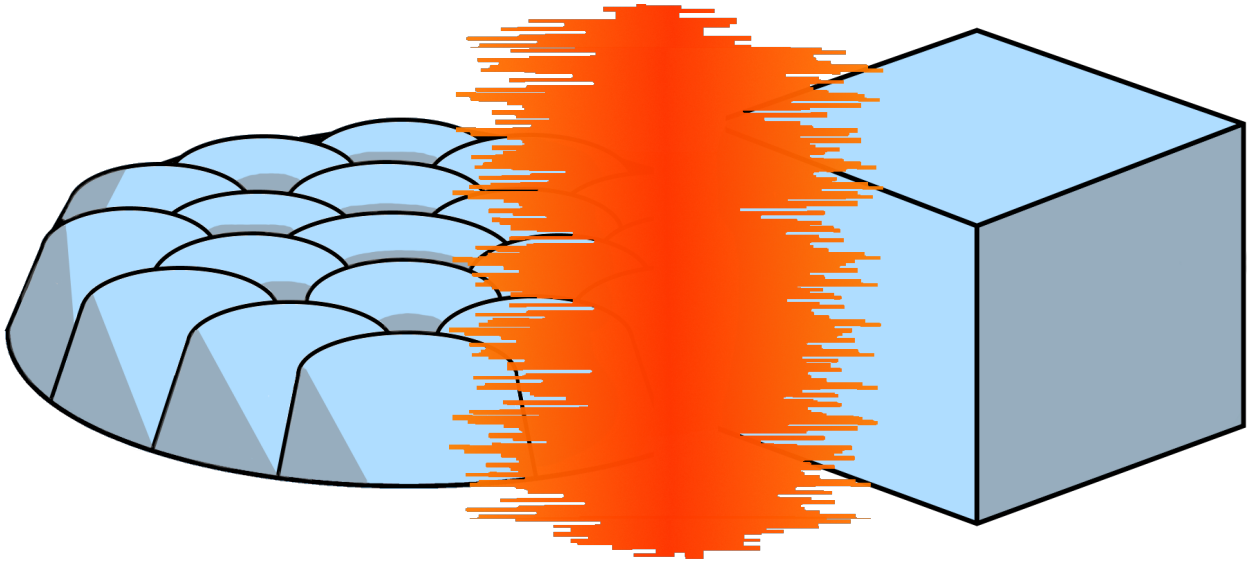

Post-Fabrication Engineering of Metal Nanoparticle Grain Structure and Faceting

For improving the fabrication of plasmonic nanoparticles for sensing and catalysis

Master's thesis in Nanotechnology

Joel Berg

Department of Physics
CHALMERS UNIVERSITY OF TECHNOLOGY
Gothenburg, Sweden 2019

Master's thesis 2019:57124

Post-Fabrication Engineering of Metal Nanoparticle Grain Structure and Faceting

For improving the fabrication process of plasmonic nanoparticles for sensing and catalysis

Joel Berg

CHALMERS
UNIVERSITY OF TECHNOLOGY

Department of Physics
Division of Chemical Physics
Chalmers University of Technology
Gothenburg, Sweden 2019

Post-Fabrication Engineering of Metal Nanoparticle Grain Structure and Faceting
For improving the fabrication process of plasmonic nanoparticles for sensing and catalysis
Joel Berg

Supervisors: Svetlana Alekseeva, Department of Physics
Examiner: Christoph Langhammer, Department of Physics

Master's Thesis 2019:57124
Department of Physics
Division of Chemical Physics
Chalmers University of Technology
SE-412 96 Gothenburg
Telephone +46 31 772 1000

Cover: Artist rendering of the transition from a top-down fabricated nanoparticle to a faceted nanocube by the means of heat treatment.

Typeset in LaTeX
Printed by Chalmers Reproservice, Chalmers Univerity of Technology
Gothenburg, Sweden 2019

Post-Fabrication Engineering of Metal Nanoparticle Particle Grain Structure and Faceting
For improving the fabrication process of plasmonic nanoparticles for sensing and catalysis
Joel Berg
Department of Chemical physics
Chalmers University of Technology

Abstract

In this thesis metallic nanoparticles of varying size and material are annealed in different temperatures for varying durations of time in order to observe how each parameter may affect the number of crystal grains in the particles. The knowledge of how different parameters affect the number of grains was then used to make single crystal particles and enhance their faceting using chemical methods. This study indicates an exponential decay in the number of crystal grains per particle as the annealing temperature is increased, with both palladium and gold particles becoming nearly single crystal when the temperature reached 0.7 of the bulk metals melting temperature. The number of crystal grains in a metal particle have also shown a linear relation to the diameter of the fabricated metal disks in the size range 100 nm-270 nm. A linear relation could be observed even when using different annealing methods and for different metals. In an attempt to enhance the faceting of the metal particles using chemical methods, nanolithography-fabricated palladium particles could be shaped into cubes, and copper disks could be grown in to larger Wulff-shaped crystals.

Keywords: annealing, grain growth, dewetting, solid state dewetting, nanoparticles, gold, palladium, copper.

Acknowledgements

There are plenty of people who have been of great importance for this thesis that deserve a big thank you. Thank you to Christoph Langhammer for being my examiner and for feedback and guidance in the project. Thank you to Svetlana Alekseeva for being my supervisor, showing me how to operate the tools used in the project and being a great support through the whole project. Thank you to Joachim Fritzsche, David Albinsson and Svetlana for producing the samples used in the experiments. Thank you to Sarah Lerch for guidance in the black magic of chemistry, making the chemical parts of the projects much easier. Than you to the people of the Langhammer group for great discussion and feedback and a thank you to the whole of chemical physics for fika and good company.

Joel Berg, Gothenburg, 2019

Contents

1
Introduction

Plasmonic nanoparticles have shown great promise as optical probes in catalysis research and for chemosensing. Palladium based nano plasmonic particles have played a key role in the of ultrafast hydrogen sensors that may pave the way for safe use of hydrogen as a fuel and energy storage [1]. Palladium forms a hydride when exposed to hydrogen, thereby changing the characteristics of the local plasmon surface resonance in palladium nanoparticles. This makes it possible for palladium nanoparticles to be used as a base for a plasmonic hydrogen sensor. One of the main problems for palladium based nanoplasmonic hydrogen sensing is the hysteresis between hydrogen absorption and desorption. This hysteresis has been reduced by the addition of gold to the palladium allowing for quicker response in hydrogen sensing [2, 3]. Corresponding tests by Alekseeva et al. have shown that the grain structure of a palladium particle also effects the hydrogen adsorption, indicating that the grain structure is relevant for the hydrogen palladium interaction [4]. Plasmonic nanoparticles have also been extensively studied for catalysis as they provide a means to monitor catalytic process on their surfaces through localized surface plasmon resonance spectroscopy. To this end, simulations have shown that the face of the material is a very important aspect in the effectiveness of the material as a catalyst, for example for the carbon dioxide dissociation on copper it has been found that face of the copper surface has a large effect on the effectiveness of the dissociation [5]. This project sets out to control and understand the grain structure and faceting of top down fabricated metal nanoparticles by post-fabrication annealing and chemical treatment of the metal nanoparticles. This combines the use of top down and bottom up nanofabrication techniques to create highly ordered structures on both a single particle and whole chip scale. Ordered structures like the ones described have been created by Preston et al. out of gold, copper, silver and palladium, which display methods that potentially could be adapted for a general set of metal nanoparticles [6]. This project largely tries to adapt the Preston et al. method with the tools available at Chalmers and elaborate on the full transition from deposited metal disk to faceted particle.

2

Theory

2.1 Annealing and its Affect on Crystal Structure

Annealing has long been used in the field of metallurgy to control the structural properties of metal. The concept that metals have crystal structures was not formulated until the 19th century when the techniques for characterising materials have become advanced enough [7]. During the following decades the understanding of annealing would expand greatly and form the basic stages of the annealing processes that are known today.
The basic mechanics of annealing is that heating the material increases the energy of its atoms and an atom with enough energy can break from its place in the lattice and move to a new location [7]. The atoms will in general migrate to a more ordered lower energy state changing the structure of the material.
This process is generally considered to happen in three stages: recovery, recrystallization and grain growth. Grain growth is the most interesting stage for this project since it aims to control the number of grains in the nanoparticles and a more in-depth theory about the grain growth can be found in section 2.1.1. Each stage works by reducing the internal energy of the material and each stage reduces the internal energy by restructuring the material. The order of the stages reflects how much strain the defects put on the lattice, with the earlier stages acting on the more straining defects.
The recovery stage is the first stage of annealing and at this stage the material's internal energy is reduced by removing linear defects from the existing grains.
Re-crystallization is the second stage of the annealing process and here the internal stresses are reduced primarily by growing new defect-free grains. This process generally leaves the metal with a finer grain structure than it had previously. These unstrained grains then expand in the grain growth stage.
This model of annealing is however based on bulk material and does not take into consideration surface effects, which are an important part of understanding the effects of annealing of nanostructures. One prominent effect observed in the annealing of nano-sized metal structures is solid state dewetting, which is further explained in section 2.1.2.

2.1.1 Grain Growth

Grain growth Is the final step of the annealing process, and in this step the grains in the metal grow by taking atoms from other grains causing a migration of the grain boundary. This process generally consumes smaller grains and produces a set of larger grains with the evolution of the average grain size depending on the time (t) and material constants σ and n, where n ranges from 0.25 to 1 [7].

$$\langle D \rangle \propto \sigma t^n \tag{2.1}$$

This is a relation that describes the grain growth during continuous grain growth, also

known as isothermal growth, in crystalline materials like pure metals [8]. This relation does not hold up for alloys, strained structures or grains annealed at very high temperatures, in which abnormal grain growth often occurs and a greater coarsening of the grains, or a second recrystallization can be observed. Abnormal grain growth lacks the clear relation that continuous grain growth has but is characterised by a large increase in the average grain size. An example of how abnormal grain growth can increase the size of grains, by Cantwell et al., is that doped Y_2O_3 had an average grain size 7 times that of non-doped Y_2O_3 when annealed for the same duration of time at 1500 °C [9]. While the requirements of common grain growth are restrictive, it is useful to have the formula of grain growth as a point of comparison to characterise the grain growth.
When looking at the continuous growth of grain structures, it is common to set n to 0.5 by default, as the value is probably close to this, and to measure the grain growth as relative grain growth from an original average grain diameter ($\langle D_0 \rangle$) forming the following relation [7, 10].

$$\langle D \rangle^2 - \langle D_0 \rangle^2 = A(T)t \tag{2.2}$$

This relation is a common simplification in the study of grain growth over time, even though n has been shown to depend on material and annealing temperature, and even change depending on the grain structure as material is being annealed [7, 11]. One of the biggest factors in annealing and grain growth is the temperature of the process, and the temperature dependence can be explained using the atomic mobility of atoms at the grain boundaries, expanding $A(T)$ to the relation below [10].

$$\langle D \rangle^2 - \langle D_0 \rangle^2 = A\frac{e^{-\frac{Q}{RT}}}{kT}t \tag{2.3}$$

A is a material constant, Q is the activation energy of the grain boundary migration, R is the gas constant and K is the Boltzmann constant. This is used by Lian et al. as a model for ultra-fine grains in Cu thin films, which is similar to the disks that are used for the experiments in this thesis [10]. Lian et al. could fit this model to the data of how the grain size of an annealed Cu thin film evolved over time. This model is for ideal grain growth of pure bulk metals, which limits the application of this model when trying to understand nanoparticles. As the particles approach single crystal regime, the model will be less accurate, but it may be used as a base in understanding the early growth in the particles. To relate the grain diameter to the number of grains in a particle, consider a disk section of an infinite plane of grains with a diameter of D_d, the average number of grains within such a disk will be as described in the equation below. This relation assumes a thin film, where the grain boundaries are vertical and can be observed from the surface of the particle.

$$g = \frac{D_d^2}{\langle D \rangle^2} \tag{2.4}$$

The combination of equations 2.3 and 2.4 above gives a model for how the grain structure of a nanoparticle can evolve with time, temperature and size of the particles, assuming continuous growth and a bulk annealing behaviour.

$$g = \frac{D_d^2}{\langle D_0 \rangle^2 + A\frac{e^{-\frac{Q}{RT}}}{kT}t} \tag{2.5}$$

With this model, the effect of annealing in nanoparticles can be compared to the model of annealing bulk material. From this it is expected that the number of grains per particle will increase with the size of the particles and decrease with the annealing time and temperature. This only covers the effect of bulk annealing, but surface effects are expected to play a larger role in the annealing of nanoparticles. One of the most notable surface effects in the annealing of thin metal films is solid state dewetting that will be explained in section 2.1.2.

2.1.2 Solid State Dewetting

Dewetting is the process when a liquid contracts and forms droplets in contact with non-wettable surface. A similar phenomenon can be observed when a thin film is deposited on a foreign substrate and is heated. The thin film breaks up into nanosized islands of varying sizes, which have been used as a method of creating nanoparticles [6, 12, 13, 14]. This retraction of the thin film is explained by the reduction of free energy by reducing the contact area between the two foreign solid materials, which in the case of metal thin films refers to the substrate and the deposited metal [15]. This causes a retraction of the metal film from the substrate, if there is enough energy in the system for the metal atoms to break from their position in the lattice and diffuse across the surface of the metal. The surface diffusion is a key difference between the dewetting of a liquid and solid state dewetting. Liquid dewetting is a bulk transport of material in response to surface interactions, while solid state dewetting only transports material by surface diffusion, which limits the scale on which solid state dewetting can be observed to the micro and nano scale as it is a surface phenomenon [15].
The process of solid state dewetting often forms facets as the atoms on a crystal plane surface require higher energy to break from their position causing formation of crystal plane surfaces on the particles [15, 16]. This makes the equilibrium shape of a solid a faceted Wulff shape compared to the round droplet of a liquid and that a dewetting annealing process of a thin film should create faceted crystals if it is run until equilibrium [14]. It has, however, been shown for Cu nanoparticles (under 1 μm in radius) that there exist nucleation barriers that prevent the breaking of existing facets and inhibit the particle from reaching equilibrium shape, while larger particles (3-5 μm in radius) could [16]. An overall expectation is that dewetted structures will form facets over time if the annealing process is continued, as has been shown by Müller et al. by annealing Au particles at 950°C between 10 min and 120 h [17]. In such a long annealing process there will however be a loss in material due to evaporation of the metal by sublimation.
Solid state dewetting is very dependent on the material of the thin film and what the thin film is deposited on, but there are trends between metals and commonly used substrates. Dewetted gold and gold alloys generally form a contact angles around 120° to 140° with common substrates like SiO_2, SiC and sapphire [13, 14, 18]. This also applies to other metals like palladium, platinum, silver and copper [6, 16, 19]. General theory about the equilibrium shape of faceted structures predicts a large contact angle for particles on a surface for metals with low wetting on the surface [20]. From the study of the adhesion of liquids to a surface the adhesion can be related to the contact angle between the surface and the liquid by the Young–Dupré equation.

$$W_{ad} = \gamma_{LV}(1 + \cos\theta) \tag{2.6}$$

In this model the adhesive energy (W_{ad}) depends on the angle between the liquid and the substrate, and the surface (θ) and the liquid vapour interface energy (γ_{LV}). The angle

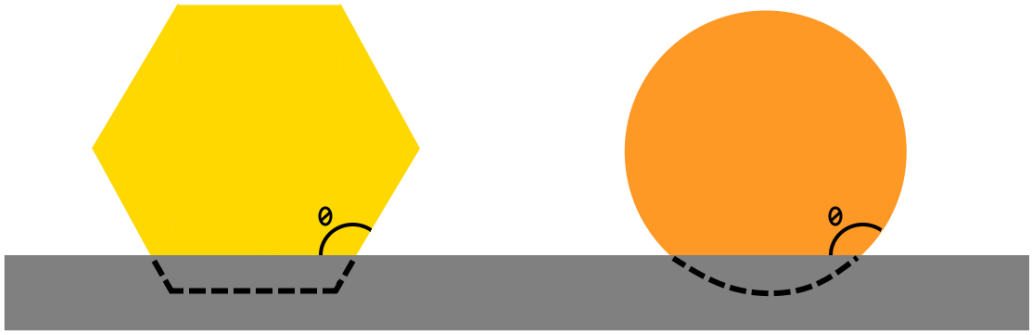

Figure 2.1: Illustration of how the contact angle between a faceted particle and a surface (left) can compare to a liquid and a surface (right).

relation to the shape of the droplet or particle can be seen in figure 2.1. This relation has been tested on the solid-solid interface and it was shown that a larger dewetted interface angle also indicates a lower adhesion in the solid-solid interface in test between Au and sapphire [14, 21]. This indicates that weaker adhesion between the metal and the substrate will make it easier to form dewetted metal structures and produces particles that protrude further from the substrate.

2.2 Scanning Electron Microscopy

A scanning electron microscope (SEM) is a tool to image very small things by using an electron beam. An SEM uses electrons accelerated to an energy of around 10 keV, which produces electrons with wavelengths of 1.22×10^{-2} nm. Because of this small wavelength the limiting factor of an SEM is how well the electrons can be focused into a single point and how well the scattered electrons can be measured. An SEM can often focus the beam to a probe of diameter 1-10 nm at the focal point [22].
An SEM takes images by using the electron probe to scan the surface of the sample and records the brightness measured at that point. All the dots form an image of the samples surface. The brightness of a point in the image depends on the angle of the surface, the material, its structure and what energy of the electrons measured with the SEM.
What electrons that are measured in the SEM is one of the most important factors in understanding the SEM images as there is a spectrum of energies of the electrons scattered from the sample. The different categories of electrons are depicted in figure 2.2. The two main modes of electrons used in SEM imaging are secondary electrons (SE) and back scattered electrons (BSE).
SEs are the electrons most often used for imaging of a surface. They are lower energy electrons below 50 eV and are generated by the inelastic scattering of the primary electrons (PE) within a few nanometers of the samples surface [22].
When the SE leave the sample surface, they are guided by a magnetic field to an Everhart-Thornley detector. The lower energy of the SE allows them to be separated from the other electrons by a magnetic field that is too weak to notably affect the high energy BSEs and

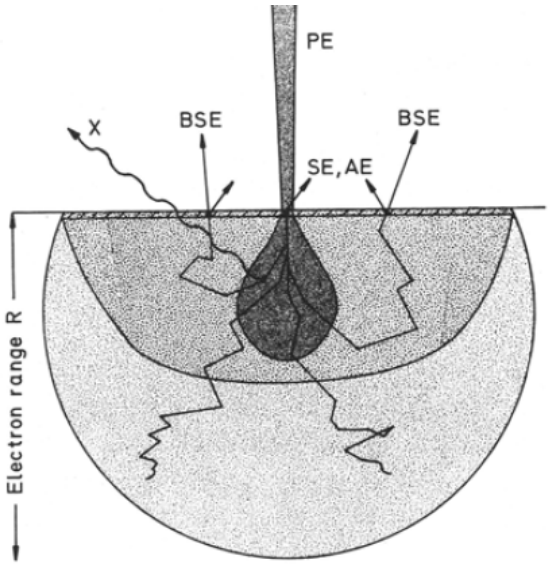

Figure 2.2: A depiction of the different electron from the SEM and their interaction of the substrate. Image by Humphreys and Hatherly [7]. The shown forms of scattered elements are primary electrons (PE), secondary electrons (SE), back-scattered electrons (BSE), Auger electrons (AE) and x-rays (X).

PEs, which allows the SEs to be separately measured. Because SEs only can come from a thin surface layer of the sample, they are a good choice for measuring the surface topology of the sample. SEs can be caused by BSEs as well as PEs and this affects the resolution and the topographic contrast, this will be further explained in section 2.2.1. Modern SEMs commonly use an in lens collection of SEs, which allows for filtering the SEs generated from PEs from the SEs generated by BSEs to produce a higher resolution image [23].
BSEs come from scattering of PEs by redirection from interaction with the nuclei of the material. The electron may be redirected multiple times within the material before leaving it and losing a bit of energy every time it does [22]. The BSEs generally leave the material at higher energy than the SEs and range in energy from 50 eV to the PEs energy (around 10 keV). The higher energy of BSEs makes them largely unaffected by the electric field that collects the SEs and they travel in straight lines. Because of BSE's interaction with the nuclei the contrast of the image is more dependent on the material than the topography of the sample. The straight trajectories of BSEs also make them show shadows of the surfaces structure. A small fraction of BSEs gets collected with the SEs because they are scattered towards the detector and contribute with a shadow and material contrast to the SE images [22].

2.2.1 Topographic Contrast

For this project, the most important role of the SEM is to show the surface structure or topographic contrast as it is also called. Grain boundaries and faceting will be visible on the surface. SEs are better at measuring the topological contrast than the other measuring modes of SEM. The following are factors regarding the surface structure that affect the topological contrast, from the book Scanning Electron Microscopy by L. Reimer [22]. 1) The SE intensity will increase with the tilt of the surface. 2) Protrusions will have an increased signal while holes have a deceased one. 3) Large surface area near the point will increase the SEs excited by BSEs and increase brightness. The impact of these factors on

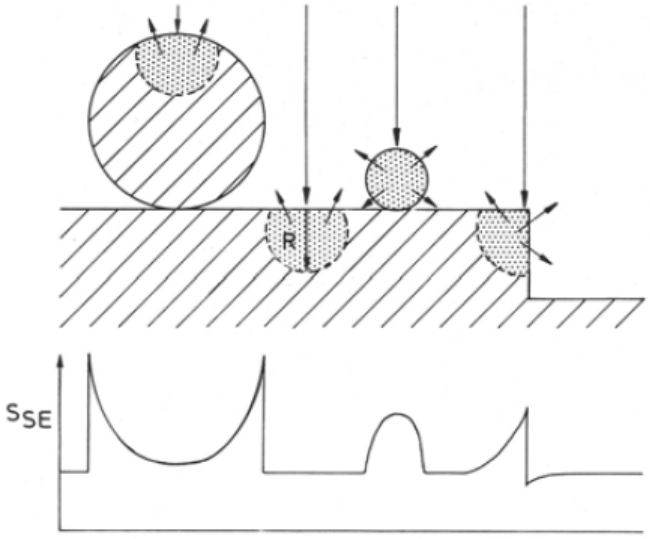

Figure 2.3: A depiction of the effects of Topology on the measured signal in SE SEM measurements. Image by Reimer [22]. The small dotted circles represent the volume where BSEs can create SEs and shows how the nearby area and feature size impact the signal strength.

simple surface shapes are Illustrated in figure 2.3.
Knowing these factors, one can expect certain patterns when looking for grains and facets in nanoparticles. For facets the edges will act like protrusions and be bright straight lines and the outline of the particles should be the brightest. The faces of faceted particles should have slightly darker shades and have slight variations in brightness due to their different angles.
When looking at structures with grains, there should be a slight shift in colour between the boundaries. There may be protrusions at the boundary making it brighter, but it will most likely not be straight like the edge of a facet. In the most extreme case, there will be a small gap between the grains, which will show up as a dark line in the SEM, as SEs have a low chance to scatter out of the gap. More grains will generally mean rougher more disorderly surface structures of the nanoparticles.

2.3 Chemical Synthesis of Nanoparticles

Chemical synthesis is an alternative to the lithographic methods of producing nanoparticles and has been employed as a method to fabricate them as early as 1857, when M. Faraday synthesised gold nanoparticles using a mixture of $HAuCl_4$ and phosphorus [24, 25]. In chemical synthesis the particles are built atom by atom by deposition from a surrounding solution of metal ions and other chemicals meant to guide the growth of the particle. With the use of chemical synthesis, one can grow particles one atom at a time, forming uniform single crystal particles and other more complex shapes [26]. The shapes of noble metal nanoparticles that have been produced include, for example, nanorods, cubes, stars and cages [27]. The base mechanics of the chemical synthesis of metallic nanoparticle is the reduction of dissolved metal salts, which causes metals in the salts to deposit onto metal surfaces within the solution [25].

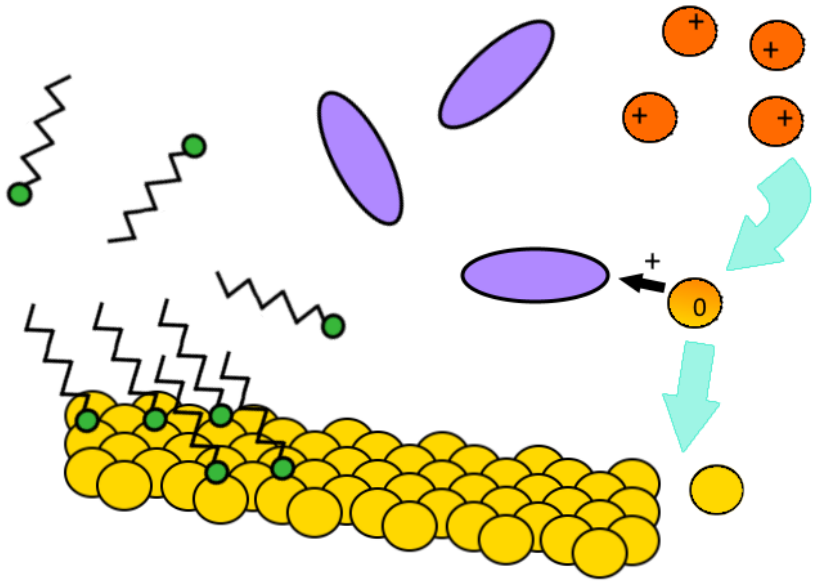

Figure 2.4: Schematic depiction of the basic principles for metal colloidal synthesis, where metal ions (orange circles) reduce to metallic atoms (yellow circles) by reducing agents (purple ovals), while surfactants (green circles with tails) attach to the synthesised surface.

The metal salts introduce metal ions into the solution, which are the building material of the nanoparticles, but these often do not spontaneously form nanoparticles. A reduction agent provides the metal ions with a way to eliminate the excess charge so it can form elemental atoms that bind to other metal atoms and build up the nanoparticle. For most reduction reactions, the reduction agent is commonly an acid [25]. Surfactants, or sometimes called as capping agents, are used to control the shape of the nanoparticles by blocking certain facets of the metal and guide the growth in other directions. Surfactants are generally hydrocarbon chains with a functionalised head allowing it to attach to a surface, with an affinity for a certain crystal plane in the case for surfactants used in the synthesis of nanoparticles [25]. The rough process of chemical metal deposition is outlined in figure 2.4.
While nanoparticles can be grown directly from the dissolved metal salts in a solution, it is common to use small colloidal nanoparticle as a seed for creating more complex structures, as it is easier to grow an existing particle than there is to generate a new one. The use of seed-mediated growth is therefore common when creating non spherical nanostructures like nanorods, or when growing nanoparticles with layers of different materials [26, 27].

3
Methods

3.1 Sample Preparation

All the experiments in this thesis were performed on samples of metal discs on a Si substrate with an intermediate layer of SiO_2 of varying thickness between the particles and Si substrate. The samples were fabricated using two different methods: hole-mask colloidal lithography (HCL) and electron beam lithography (EBL). HCL uses a solution of colloids to coat the substrate and form a mask for lift-off processing and results in a set of randomly ordered discs that have nearly the same diameter as the colloids and corresponding size distribution [28]. EBL uses a beam of high energy electrons to expose a resist that is sensitive to high energy electrons to make a pattern with very fine resolution. In contrast to HCL, the resulting discs have very narrow size distribution.
The samples used for studying how temperature and time effect the grain structure were made using HCL and colloids with a nominal diameter of 250 nm and for later experiments a nominal diameter of 147 nm. The fabricated thickness of metal disks were 30 nm for Pd, 3 nm of Au with 27 nm of Pd on top for Pd with 10% Au, 24 nm for Au and 30 nm for Cu. This process is visualised in figure 3.1 and was done by using the following recipe.

1. Spin coat a layer of PMMA of molecular weight 950,000 g/mol on to the substrate using a rotational speed of 2000 rpm for 1 min.
2. Soft bake the PMMA coated substrate, to harden the PMMA, at 170 °C for 10 min.
3. Etch the surface of the PMMA with oxygen plasma at 50 W for 5 s to make the surface more hydrophilic.
4. Apply charged polyelectrolyte fluid of 0.2 wt.% PDDA to build charge on the surface for the colloids to attach to.
5. Carefully rinse off excess polyelectrolyte fluid and dry the surface with N_2.
6. Apply the colloidal solution of polystyrene beads to the substrate and allow the colloids to attach to the surface using the difference in charge between the surface and the colloids.
7. Rinse off the excess colloidal solution and dry the sample with N_2.
8. Deposit a thin layer of about 20 nm Cr on the coated substrate to form a plasma etching resistant layer on the PMMA.
9. Peel off the colloids using tape to form holes in the Cr layer, completing the mask.
10. Etch down the PMMA in the exposed holes with 50 W oxygen plasma to remove the PMMA in the holes left after peeling off the colloids.
11. Deposit the metal of the nano-discs on the masked substrate.
12. Lift off the mask by dissolving the underlaying PMMA in acetone leaving only the metal deposited in the hole on the substrate.

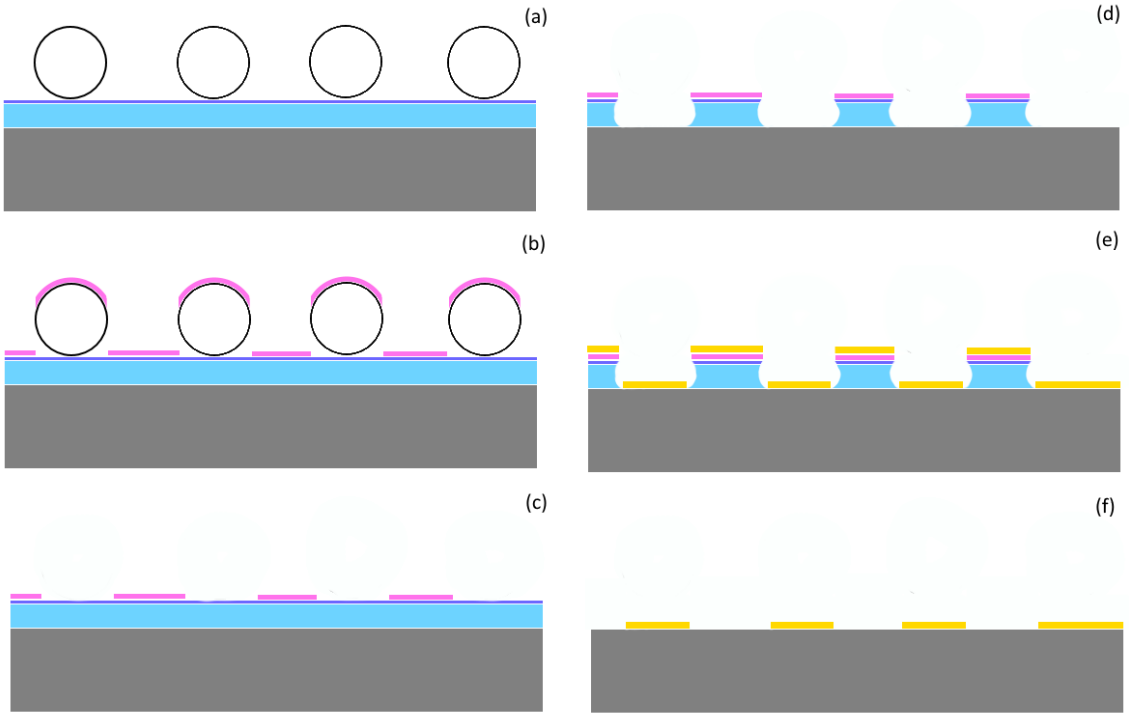

Figure 3.1: Step-by-step visualisation of HCL. a) deposition of PMMA, PDDA and colloids, b) Cr-mask deposition, c) striping the colloids, d) Etching the exposed PMMA, e) depositing metal, f) lift off the remaining PMMA.

The substrate was then diced into 7 by 7 mm samples on which different annealing tests were done. This method yielded many particles with the same size with a cheap fabrication process. The distribution of diameter of the fabricated particles can be seen below in figures 3.2 and 3.3.

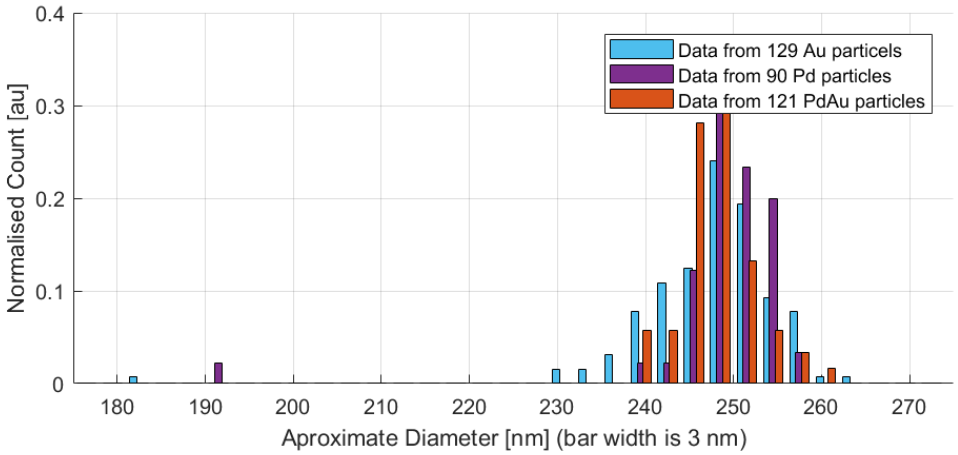

Figure 3.2: The size distribution of particles fabricated using 250 nm colloids in HCL.

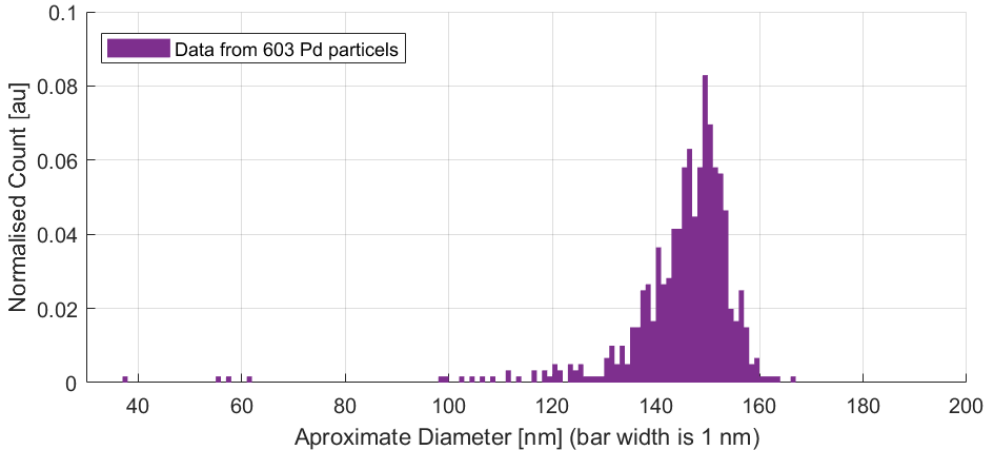

Figure 3.3: Distribution of particle size of Pd particles fabricated using 147 nm colloids in HCL.

The EBL samples where made on Si substrate with a 60 nm layer of SiO_2 between the Si and the particles on the substrate. In this process the electron beam is used to crosslink the PMMA to make it resistant against solvents [29]. The two layers of resist in this process are used to form an undercut as the top layer is more sensitive to the electron beam. This causes the patterned area to be undercut making lift-off process of the mask easier. The following recipe was used for the EBL fabrication:

1. The substrate was spin coated with MMA(8.5)MMA using a speed of rotation of 3000 rpm for 1 min with 2 s acceleration time.
2. The substrate was then baked at 180 °C for 5 min.
3. The sample was the spin coated with PMMA of molecular weight 950,000 g/mol using a speed of rotation of 3000 rpm for 1 min with 2 s acceleration time.
4. Another baking at 180 °C for 5 min was then done to soft bake the PMMA.
5. The resist was then patterned and exposed the area around the holes crosslinking the PMMA using EBL.
6. Remove the non-exposed PMMA in the holes with acetone forming the mask.
7. Then deposit the metal to the desired thickness.
8. The mask is then removed by etching using oxygen plasma leaving only the metal disks left on the substrate.

3.2 Annealing Methods

In this project multiple furnaces with different annealing recipes were tested to determine how they can be used to control the grain structures of the nanoparticles. In the sections bellow are descriptions of the different tools used for annealing and descriptions of the operating process.

3.2.1 Thermolyne Furnace

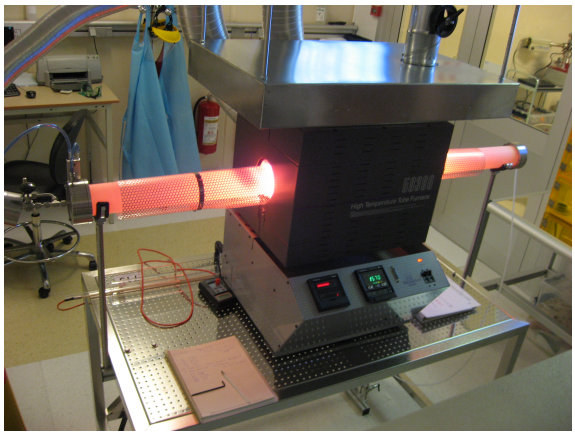

Figure 3.4: Image of the Thermolyne furnace

One of the furnaces used is a Thermolyne furnace noted in the myfab LIMS system as Thermolyne - Open Tube/1600 °C and seen in figure 3.4. In this furnace samples were slowly heated to a set temperature in a ceramic crucible held at that temperature for a while and then allowed to cool ambiently. This furnace could go to a higher temperature (1600 °C) than any other furnace used in these experiments but had a very slow rate of heating which greatly limits how many different annealing times and temperatures that could be tested. The set temperature and the holding time was varied in the use of this furnace and the general steps in using the furnace was as follows.

1. Place sample in the crucible and push the crucible in to the centre of the furnace tube and then close the tube.
2. Turn on the Ar flow to about 0.6 L/s.
3. Heat the samples by 5 °C/min to the set temperature.
4. Hold the temperature for a set holding time.
5. Turn off the heat and let it cool ambiently.
6. When the machine has cooled, turn off the gas flow and remove the samples.

3.2.2 JIPELEC JetFirst 200

The Jipelec JetFirst 200 (figure 3.5) is a tool for rapid thermal processing (RTP) and it was used to test how short bursts of high temperature would affect the nanoparticles. The JetFirst produces heat by radiating the sample, laying on a raised graphite plate, with a large amount of light from a 16 kW set of lamps above the sample while under a controlled gas flow.
The limits placed on the tool by responsible personnel were: no process above 900 °C, not to heat faster than 10 °C /s and not to hold at set temperature for longer than 15 minutes. All tests were done within these restrictions. The gas used in the processing was argon in order to try limit oxidation of the particles.
The steps of the RTP were as follows, where the set temperature and the holding time varies:

Figure 3.5: Image of the Jipelec JetFirst 200

1. Place the samples as close to the centre of the graphite plate as possible.
2. Vacuum pump the chamber for 20 s.
3. Open the purge valve for 30 s.
4. Vacuum pump the chamber for 20 s.
5. Flush the chamber with 2000 ml/s gas flow of Ar for 20 s.
6. Ramp up the heat at a rate of 10 °C/s from a base set temperature of 0 °C to the set temperature under a 1000 ml/s Ar gas flow. While the reel temperature started at room temperature the set temperature starts from 0 °C.
7. Let the sample sit at the set temperature for a set holding time under 1000 ml/s Ar gas flow.
8. Turn off the heat.
9. Let the sample cool for 4 to 8 min under 2000 ml/s Ar gas flow.
10. Wait the required minimum of 4 minutes or until the thermocouple in the RTP reaches 85 °C.

An important note about the Jipelec JetFirst 200 is that it measures the temperature from the bottom of the graphite plate on which the samples sit. Since the sample is directly heated by the light from above the sample it may experience a higher heat than the thermocouple below the graphite plate which is used to regulate the temperature.

3.2.3 Lab Furnace

The Annealing reactor in the lab is a newly refurbished annealing reactor that was assembled at the department. The furnace is a small tube furnace, depicted in figure 3.6 with the central part being an isolated glass tube with a heating coil. The heating coil is connected to the power supply and the temperature is regulated with a thermocouple in the reactor so it can maintain a steady temperature.
The reactor takes in a set temperature and tries to maintain it by controlling the heat applied to the reactor. The reactor has no active cooling and relies only on ambient heat diffusion for cooling the reactor. The steps of operation of this furnace were as follows where the set temperature and holding time were varied:

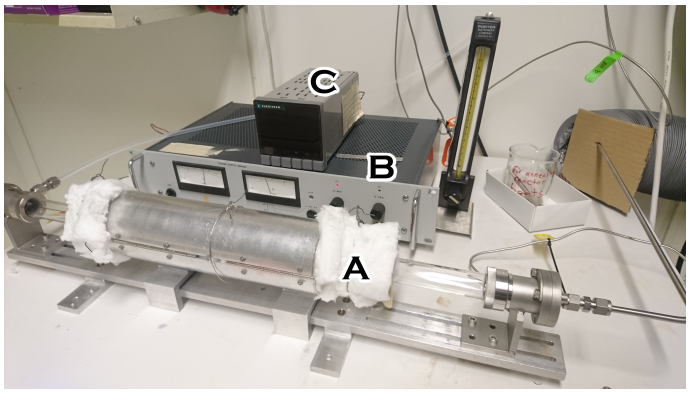

Figure 3.6: Image of the annealing reactor in the lab with the different parts being: A) glass tube with heating coil wrapped in insulating material, B) power supply and C) temperature controlling unit.

1. Place samples in a crucible in the centre of the reactor.
2. Flush the chamber with a gas flow of 96% Ar and 4% H_2 at a rate of about 0.3 L/min.
3. Start the heater and let it heat to the set temperature as fast as possible. This took about 15 to 30 minutes depending on set temperature.
4. Let the sample sit at the set temperature for a set holding time.
5. Turn off the power supply to stop the heating and let it cool ambiently.

3.3 Chemical Processing of Nanoparticles

To enhance the faceting of particles a chemical method adapted from Preston et al. was used [6]. For all the chemical processes 10 mL beakers were used to hold the mixtures. The heating was done by directly placing the beaker on a hotplate and heating to near the desired temperature. The samples were left on the hotplate during the growing process. The following chemicals where used in the faceting of the particles, different chemicals were used for different metals as can be seen in the recipes below. Ascorbic acid (AA) was used as a reducing agent while Centrimunium bromide (CTAB) was used as a capping agent. Polyvinylpyrrolidone (PVP) was both used as a capping agent and a reducing agent. The metal salts used for Pd, Cu and Au particles respectively were H_2PdCl_4, $Cu(NO_3)_2$ and $HAuCl_4$. A rough visualisation of the process can be seen in figure 3.7.

1.

To enhance the faceting of the Pd particles the following recipe was used:

1. Mix an aqueous solution of 3 mL AA (25mM) and 1 mL of CTAB (200 mM).
2. Heat the solution of surfactants and reducing agent to about 40 °C under a cover by letting it sit on a 70 °C hotplate.
3. Place the sample in the heated solution and leave it to incubate with the surfactants for 1 min.
4. Initiate the reaction by rapidly adding 1 mL of room temperature aqueous H_2PdCl_4 (2 mM).
5. Let the seed sit in the solution for 15 min under cover.
6. Then remove the sample, rinse it, sonicate it in DI water and dry it with an N_2 gun.

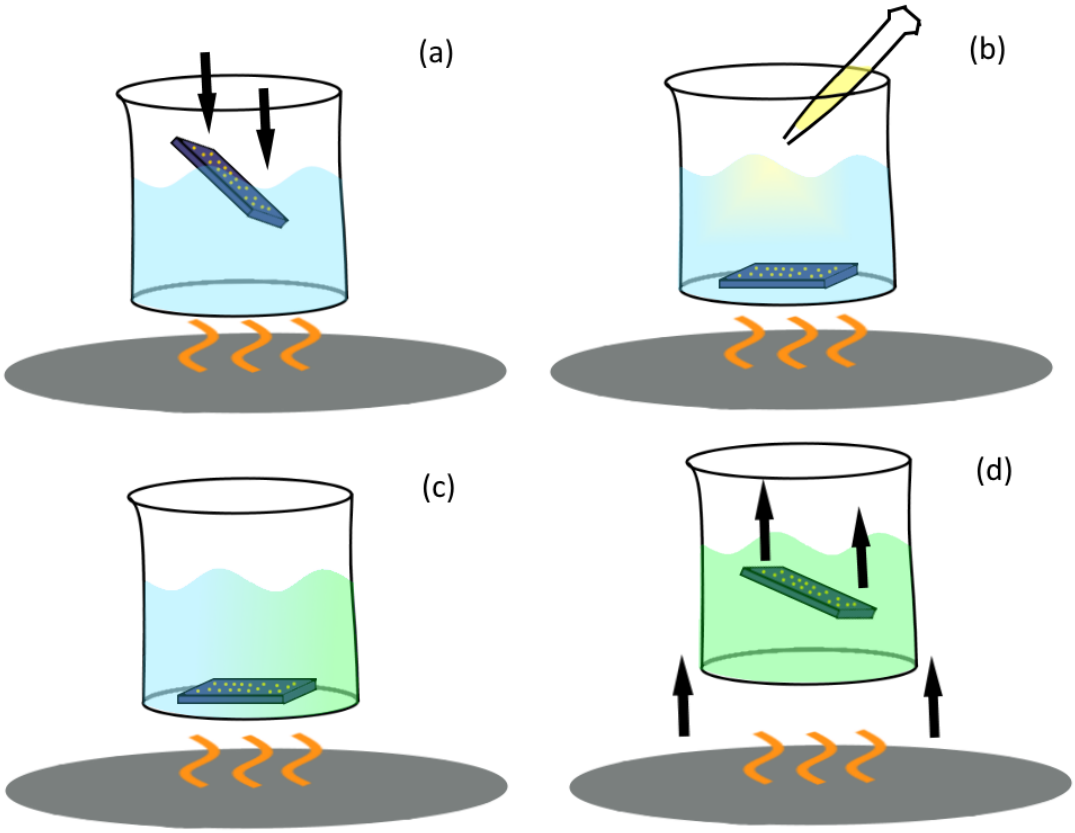

Figure 3.7: Visualization of the chemical treatment. a) The samples are added to the heated solution of surfactants and reduction agent. b) The metal salts are added to start the growing process. c) The sample is left to grow with changing color of the solution as the metal salts are reduced. d) The beaker is removed from the hot plate and the sample is removed from the beaker to be cleaned.

The Cu particles had a shell of copper oxide on the surface that first needed to be removed before the chemical growth. To enhance the faceting of the Cu particles the following recipe was used:

1. Place the sample in borohydride (10 mM) for 3 min.
2. Place it in nitric acid (5 mM) for 4 min.
3. Put the sample in 1 mL of ascorbic acid (10 mM) near boiling on a 220 °C hotplate under a cover for 1 min.
4. Start the growing process by quickly adding 3 mL of $Cu(NO_3)_2$ (1 mM) and let the particles grow for 5 min.
5. Finally, rinse the sample, sonicate it in DI water and dry it with an N_2 gun.

To enhance the faceting of the Au particles the following recipe was used:

1. Heat 4 ml of PVP solution (1 mM) to near boiling temperature by letting it sit on a 220 °C hotplate.
2. Put in the sample and let it sit in the heated PVP solution for about 15 to 30 s.
3. The reaction was then initiated by injecting 1 ml of room temperature $HAuCl_4$ (1 mM).
4. Let the sample sit in the growth solution for 4 min.
5. Remove the sample from the solution, rinse it, sonicate it in DI water and dry it with an N_2 gun.

3.4 SEM Measurements and Image Analysis

The SEM used to measure the nanoparticles in this project was a Zeiss Supra 60 VP. The SEM was operated with a working distance of 4.5 mm, a primary electron energy of 15 keV in the InLens electron capture mode which primarily capture back scattered electrons. The 4.5 mm working distance is chosen to be just above the closest safe working of 4.0 mm recommended for the tool by responsible personnel. The use of the higher energy of 15 keV gives a higher resolution than lower energies at the cost of deeper penetration of the electrons in the sample. The deeper penetration work to the benefit of detecting the grain boundaries of the particles as they go through the whole particle. The use of a silicone substrate helps with dissipating the electrons that penetrate the sample and reduces the amount of built up charges that may disturb the imaging in the SEM.

3.4.1 Particle Size Measurement

The image processing software imageJ [30] was used to get the size distribution of the particles using the fact that the edges of the particles are brighter than the surrounding surfaces in SEM. By setting a brightness threshold and letting everything above it be considered as a particle, the built in Particle finder in imageJ can deduce what in the image are particles and what the areas of the particles are. Below is a detailed description of how this is done and how the data is processed.

The process starts with an SEM image of the particles, as one seen in figure 3.8.A. The image is then converted to an 8-bit grey-scale image by selecting from the ImageJ menu Image>Type>8-bit. Then open the threshold menu in Image>Adjust>Threshold, check dark background and adjust the threshold until at least the outline of the particles are red, but preferably the whole particle, as seen in figure 3.8.B. Next the Scale of the image was set by going to Analyse>Set Scale and inputting the how many nanometers each pixel was. For an image with 100k magnification the SEM tif-file had a pixel size of 3.496 nm by 3.496 nm. Finally, the particles were found using Analyse>Analyse Particles where It

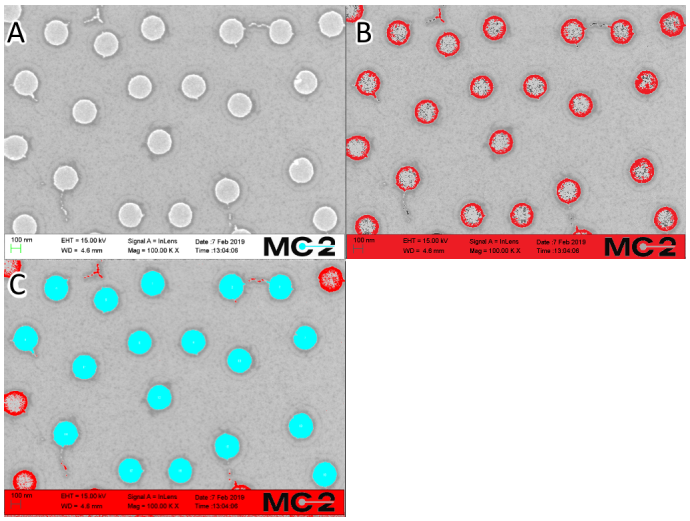

Figure 3.8: In these images the process of getting the area of each particle is visualised. A) The original SEM image of the particles. B) The colour threshold is set so that the outlines of the particles are coloured red. C) The areas identified as particles are coloured blue.

was set up to detect particles between 10,000 nm^2 and 300,00 nm^2, show an overlay mask, exclude particles on the edges and include holes in the particles. This yields the area of each particles in the image and displays them as an overlay on the image as can be seen in figure 3.8.C. The data was saved to a txt file and loaded into MATLAB where the area was converted to an approximate diameter using the formula for a circles area for easy comparison.

3.4.2 Grain Measurement

The grain measurements use a very similar process to the particle size measurement. Firstly, a map of where the particles are was taken in exactly same way as the particles where measured for the size. Then the brightens and contrast of the image was adjusted to highlight the features within the particles. The grain boundaries were then identified by hand and marked with a black line in order to create clear separation of the grains. To make the grain boundaries clearer, the contrast of the image was increased to better see the more subtle differences in the grains. After the grain boundaries have been marked this way one can use ImageJ particle detection software to identify the grains as particles and take the position of every grain. The detection of the grains used a smaller threshold size of what counted as a particle. In general, this lower size was near 500 nm^2 instead of the 10,000 nm^2 used for whole particles but this varied depending on the size of the grains where smaller size thresholds where use to detect finer grains.
This data could be loaded into MATLAB and where for each particle the program identified which grains were within which particle and made a distribution of the number of grains per particle.

4

Results

The number of grains per particle formed a distribution, on every sample, that closely resembled a Poisson distribution. A modified Poisson distribution of the likelihood that a random particle will have n number of grains has therefore been adapted to the data.

$$P(n) = \frac{(\lambda - 1)^n}{(n-1)!} e^{-(\lambda - 1)} \tag{4.1}$$

This modified Poisson distribution, where the smallest value is one instead of zero, shows a very high resemblance to the measured distribution of the particles, as can be seen in figure 4.1
The only input needed to plot this distribution is the mean number of grains per particle (λ) which means that the whole distribution can be represented by the mean value. Because of this the mean value is the primary thing that is needed to track in relation to the factors affecting the grain distribution of the nanoparticles.

4.1 Controlling the Grains

4.1.1 Temperature Dependence

The temperature has shown itself to be the most effective way of reducing the number of grains, as large changes to the number of grains occur when the temperature is changed within only one order of magnitude. Bellow one can see how a set of Au particles were affected by different annealing temperatures when annealed for the same duration of time. These samples where 250 nm in diameter Au disks made using HCL and heat treated in the jipelecRTP as described in section 3.2.2 with a 15 min annealing time in temperatures ranging from 360 °C to 900 °C. The annealed particles and the distribution of grains per particle can be seen in figure 4.2 and 4.3 respectively.
The Initial tests over temperature were done in the temperature range of 600 °C to 900 °C as higher temperatures were more promising for getting single crystals. In this range there was a clear decline of the number of grains for particles of Pd and Pd with 10% Au but nearly constant number of grains just above 1 for Au, as can be seen in figure 4.4. The idea of changing the temperature axis from degrees Celsius to absolute temperature relative to the materials melting temperature was inspired by structure zone diagrams which show grain structure over a relative temperature [31]. In the relative temperature the range of 600 °C to 900 °C covered 0.47 to 0.64 of the relative temperature for Pd and 0.66 to 0.88 for Au. There where therefore no overlap in the relative temperature of the plots in this temperature range but they nearly had an equal point in the 0.64 and 0.66 relative temperatures. In relative temperature the Pd and Au data from the 600 °C to 900 °C range looked like it could form a single continuous curve, and this gave inspiration to further tests of different temperatures.

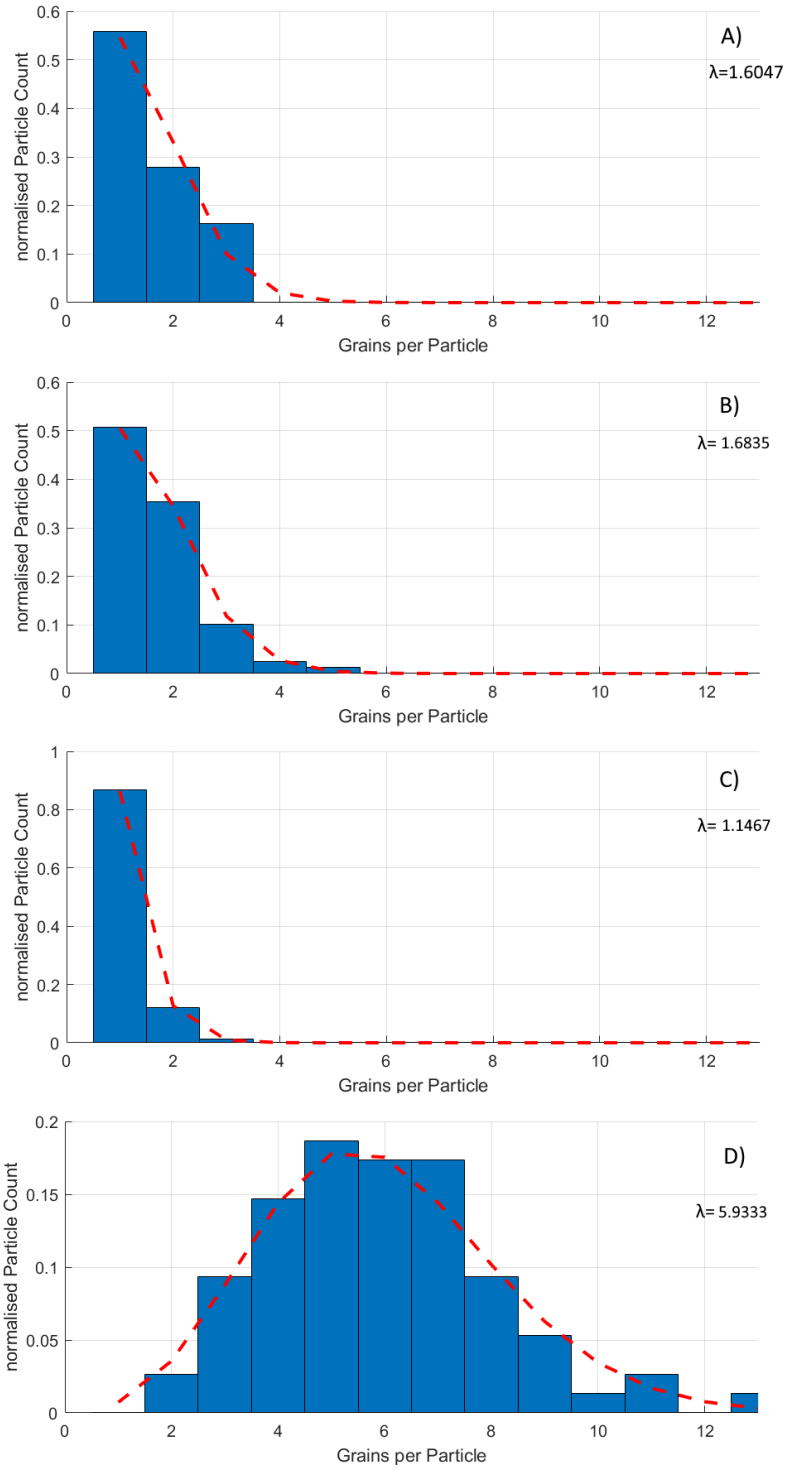

Figure 4.1: Examples of how the distribution of grains per particle look like for a single sample. The red dashed line is an adapted Poisson distribution (see equation 4.1) based on the mean value (λ) of the number of grains. A) Pd particles annealed at 500 °C for 24 h in the Lab Furnace. B) Pd with 10% Au annealed at 600 °C for 24 h in the Lab Furnace. C) Au particles annealed at 600 °C for 15 min in the RTP reactor. D) Au particles annealed at 360 °C for 15 min in the RTP reactor.

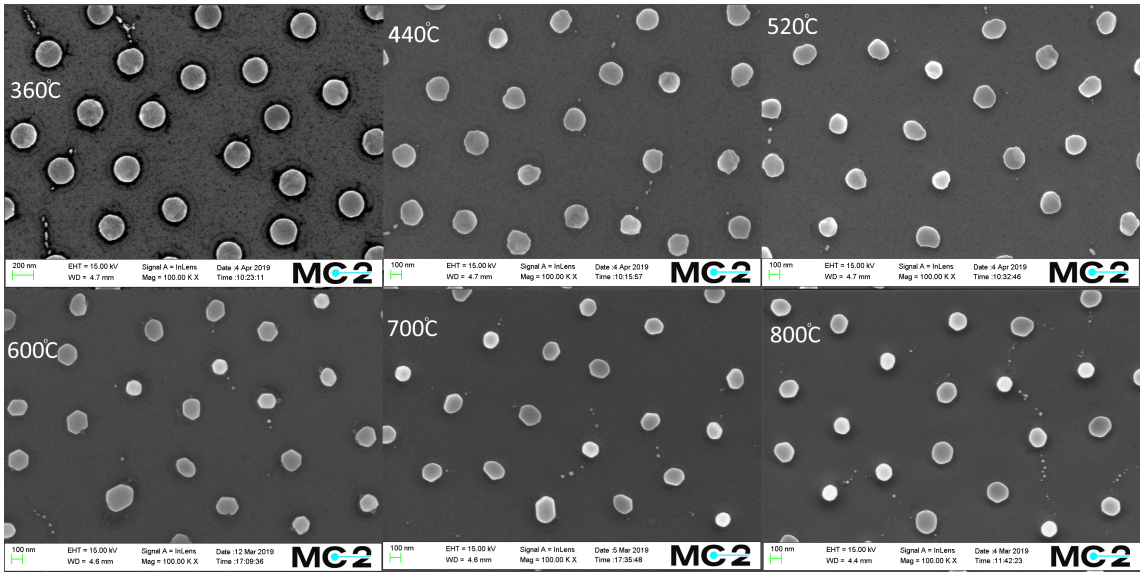

Figure 4.2: Here are SEM images at 100kx magnification for gold particles annealed for 15 min at the temperatures indicated in the images.

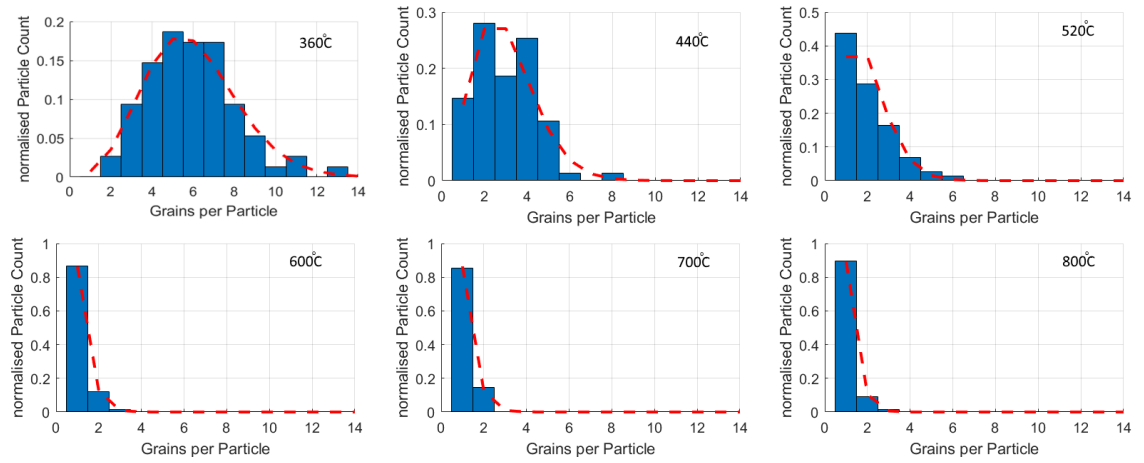

Figure 4.3: These are the distributions of the number of grains per particle of the same samples that are imaged in figure 4.2.

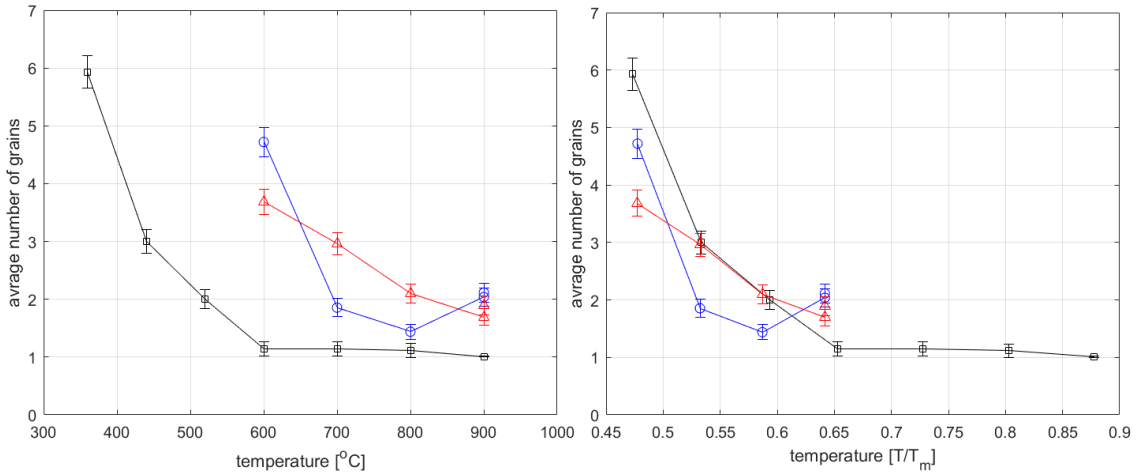

Figure 4.4: This is how the average number of grains change over temperature for 250 nm in diameter nanoparticles of Au (black squares), Pd (red triangles) and Pd with 10% Au (blue circles) annealed by RTP for 15 min. Temperature given in Celsius in the left image and relative temperature on the right.

The next step was to match the relative annealing temperatures of Au and Pd to compare them and 600 °C, 700 °C and 800 °C for Pd corresponded to 360 °C, 440 °C, and 520 °C annealing temperatures for Au. With these tests a much clearer curve could be seen for the number of grains in Au and the curve followed the same trend as Pd.
The curve for the Au grains in figure 4.4 looks like an offset exponential curve decaying toward 1 instead of the normal decay towards 0. If it is exponential it should form linear relation when you take the natural logarithm of the average number of grains minus one. This is shown in figure 4.5 with a linear fit to the Au grain data. This fit has the form:

$$ln\left(\lambda\left(T\right)-1\right)=\left(8.0-13.9T\right) \tag{4.2}$$

Which means the function of the average number of grain for each particle for this process can be expressed as:

$$\lambda\left(T\right)=1+e^{\left(8.0-13.9T\right)}. \tag{4.3}$$

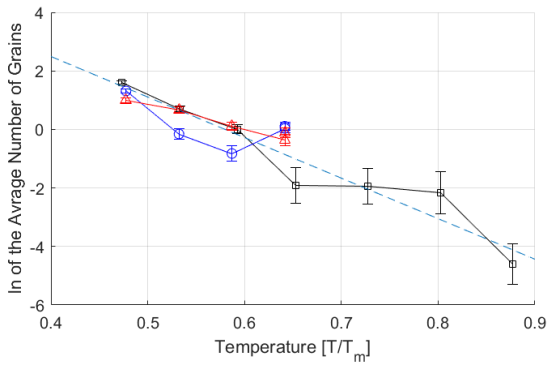

Figure 4.5: The natural logarithm of the data from figure 4.4 with a fit to the Au data with a function of $ln\left(\lambda\left(T\right)-1\right)=\left(8.0-13.9T\right)$

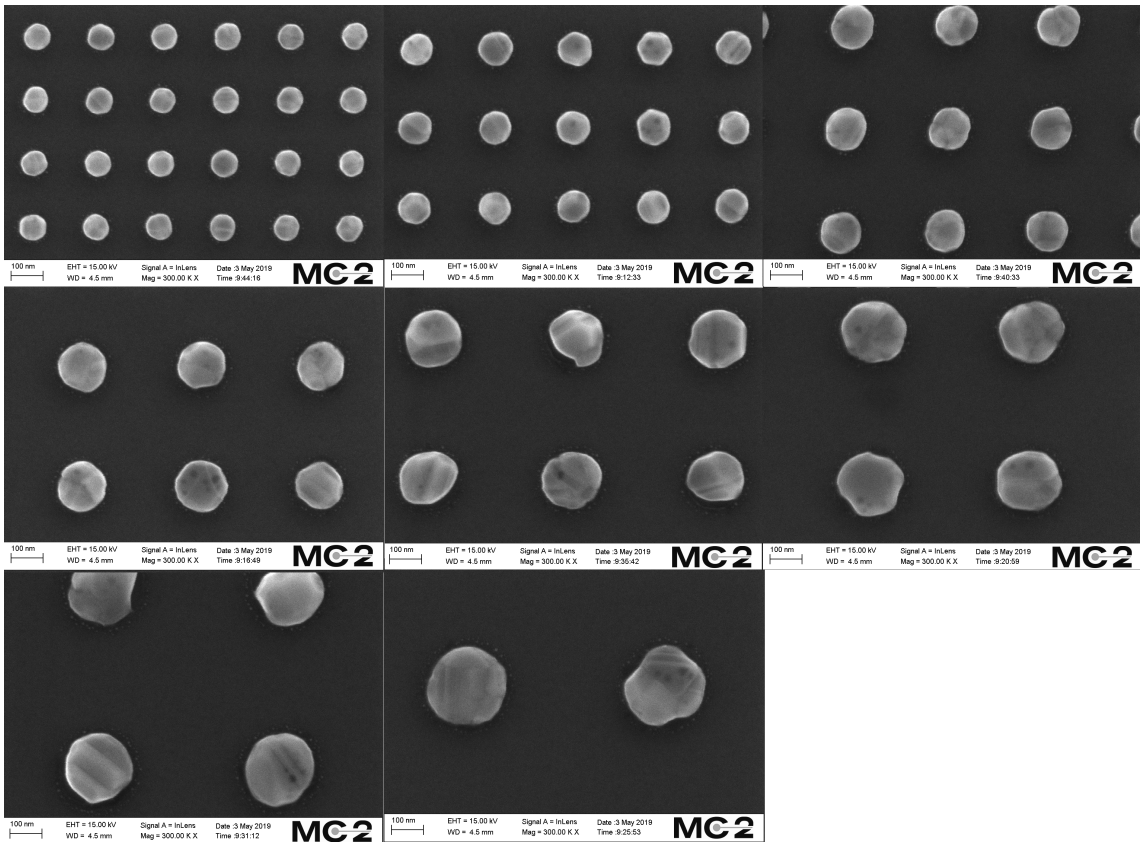

Figure 4.6: These are a set of SEM images of EBL fabricated Pd particles of different fabrication sizes ranging from 100 nm to 270 nm annealed for 24 h at 500 °C. Every image has the same magnification at 300kx. The variation of the average number of grains over the fabrication size can be seen in figure 4.7

4.1.2 The Size and Shape of Particles

To test how the size of the fabricated disks affect the number of grains in the particles, samples with arrays of different diameter disks where fabricated using EBL for the annealing experiments. All the samples tested indicated a linear relation between the average number of grains in the particles and the diameter of the fabricated disks as shown in figure 4.7. This relation is to hold true even when changing the particle material and the method of annealing.
A notable change that can be observed in the shape of the particles in figure 4.6 is that they get rounder as the they get smaller and have fewer grains. A similar trend can be observed in figure 4.2 where the lowest temperature corresponds to round particles with many grains and the shape gets odder as the temperature increases. However, when it reaches the highest temperatures it forms the rounder dewetted structures and returns to the rounder shape. The partially dewetted particles become odd shapes and the round shapes are achieved by non-dewetted and fully dewetted particles.

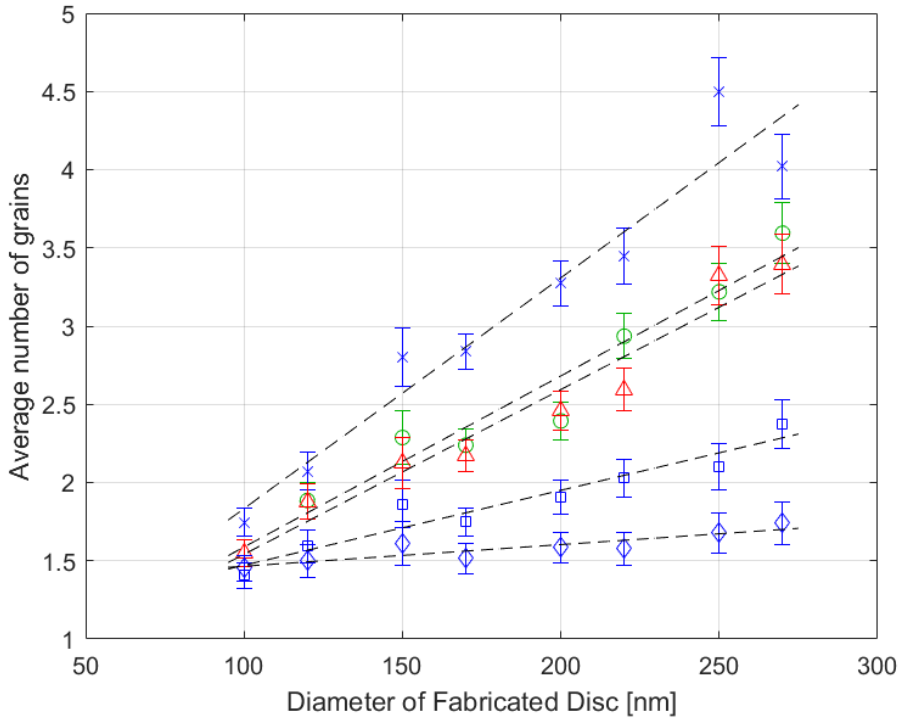

Figure 4.7: A graph of how the average number of grains in the particles changes with the size of the original disk. The lines are linear fits of the data from particles annealed with the following procedures: Pd at 500 °C for 24 h (blue X's, correspond to SEM images in figure 4.6), Pd with 10% Au at 500 °C for 24 h (green circles), Au at 440 °C for 15 min (red triangles), Pd at 700 °C for 15 min (blue squares) and Pd at 900 °C for 15 min (blue diamonds).

A notable difference in the shape of the particles is between EBL and HCL fabricated samples that can be seen in figure 4.8. Here we can see a set of particles of the same fabrication size and that have gone through the same annealing process. In these particles the EBL fabricated particles form rounder and more uniform particles compared to the HCL fabricated particles. This indicates that for the EBL fabricated samples it is easier to form dewetted structure.

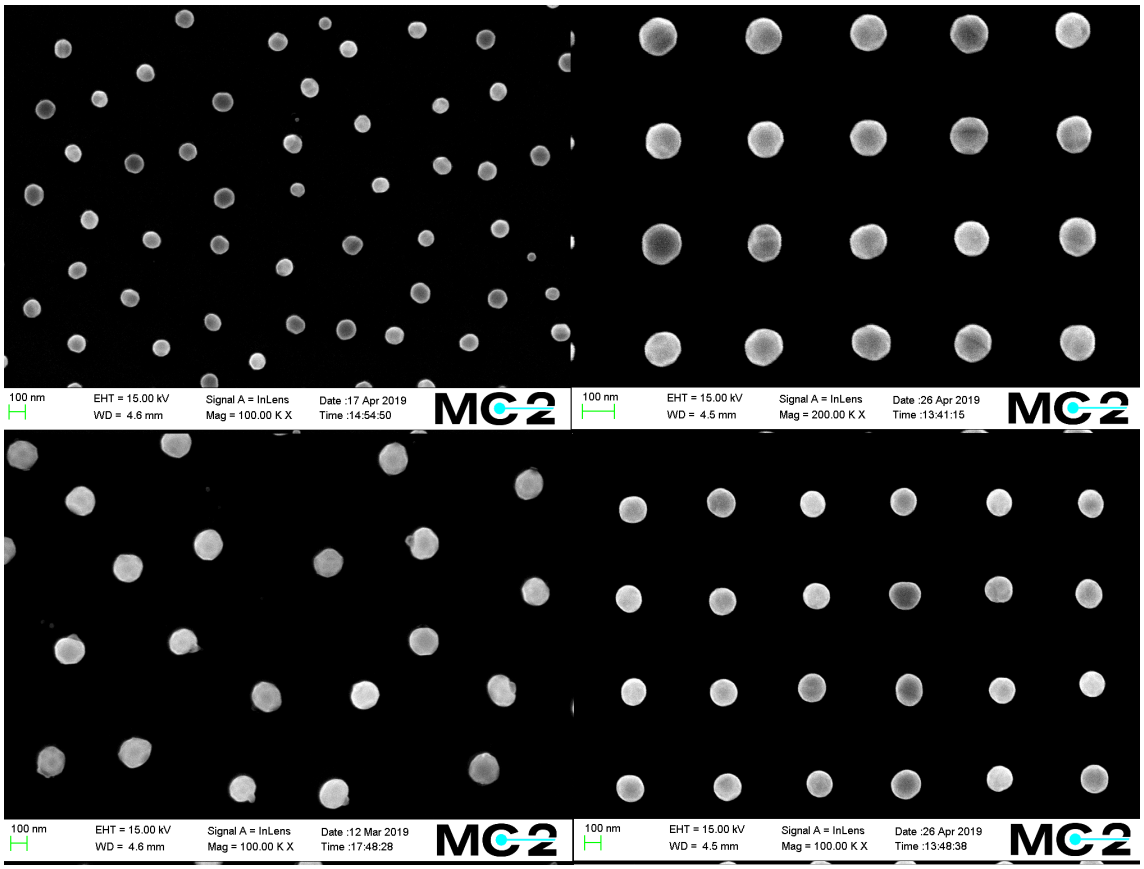

Figure 4.8: These are four SEM images of Pd nanoparticles that have been annealed for 15 min at 900 °C. The left side are HCL samples while the right side are EBL samples, the top images are both from about 150 nm in diameter fabricated discs while the bottom two are originally 250 nm fabricated discs.

4.1.3 Time dependence

The number of grains in a particle have weaker dependence on time compared to temperature but there is a reduction in grain number over time as can be seen in figure 4.9. While the time scale for the annealing differ greatly with temperature, it appears that for temperatures bellow 500 °C it will take over 24 h for Au and Pd to reach single crystal. Note that each point in the plotted lines is the data from a different sample the data does not show how a single sample evolve over time.

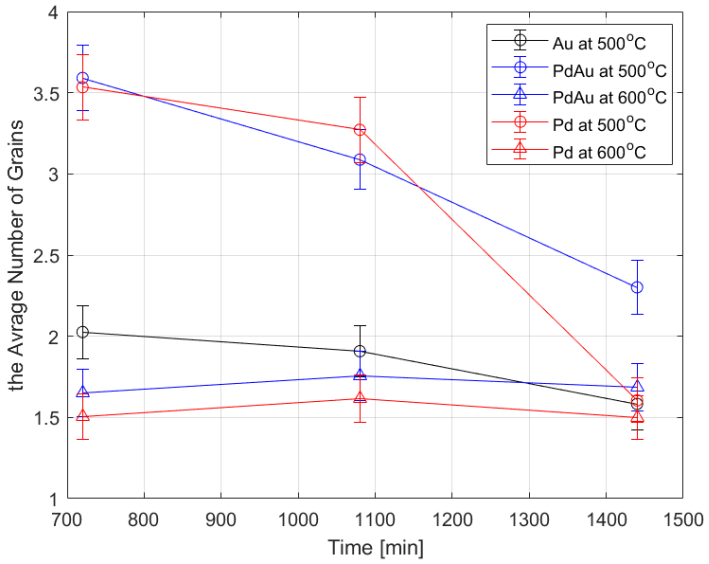

Figure 4.9: A graph of how the average number of grains change with the annealing time in the Lab furnace. The samples where annealed at the temperature shown in the legend.

4.2 Chemically Enhanced Faceting

The most successful attempts at faceting can be seen in figure 4.10 and it shows enhanced faceting of Cu and Pd particles. The Cu particles used were 250 nm HCL disks annealed at 900 °C for 1 min and the Pd particles used were EBL particles of varying size that were annealed at 900 °C for 15 min. On the Cu particles before the chemical process, in the upper left image in figure 4.10, one can see tint around the particles. This tint is most likely a thin oxide which would need to be, and was, removed before any copper could be grown on the particles.
The result for the chemical process on the Au particles, which can be seen in figure 4.11, where not as clearly defined as those for Cu and Pd. The difference between the particles before and after is subtle, the flatter structures look like they act as a plane on which a faceted particle seems to grow as the edge facets become larger after the chemical process. The Cu particles grew a lot to what looks like a Wulff-shape for the more uniform particles but have a very notable variation in size and shape. The Pd particles grew to a square like structure and as CTAB blocks the {100} face of FCC metals the cube could be a completely grown cube of {100} faces. The concentration of metal salts played in critical role in how the particles faceted and we could see this clearly when initial tests on Pd turned out with mostly small spiky growth. Increasing the concentration brought the particles closer to a clear faceted shape as can be seen in figure 4.12.
The particles fabricated using EBL samples had a high tendency to drop of the substrate when they went through the chemical process. Partial drop off could be seen in the Pd particles, see figure 4.13, and all EBL Cu particles that where tried for the chemical treatment dropped off.

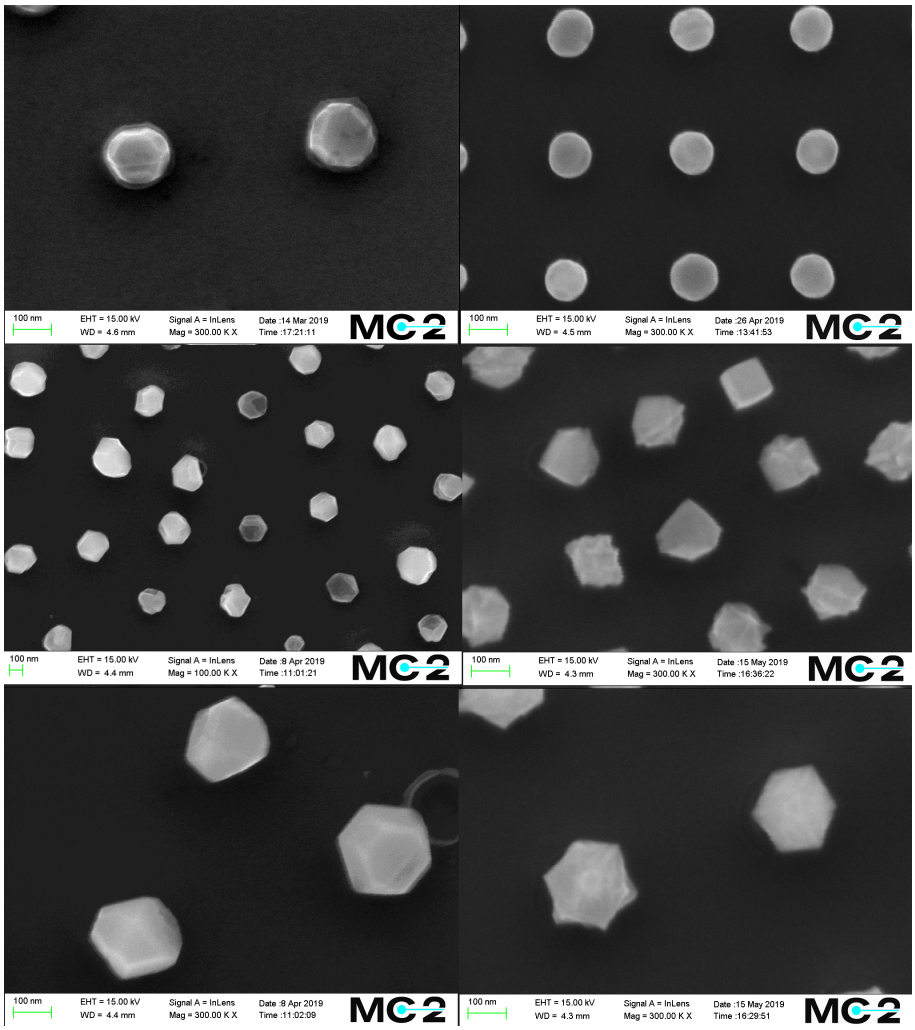

Figure 4.10: These SEM images show how the chemical process can affect the particles of the Pd on the right and Cu on the left. The first row is a set of annealed particles before they were used fore chemical enhancement of faceting and the rows bellow show how the particle looks after the treatment.

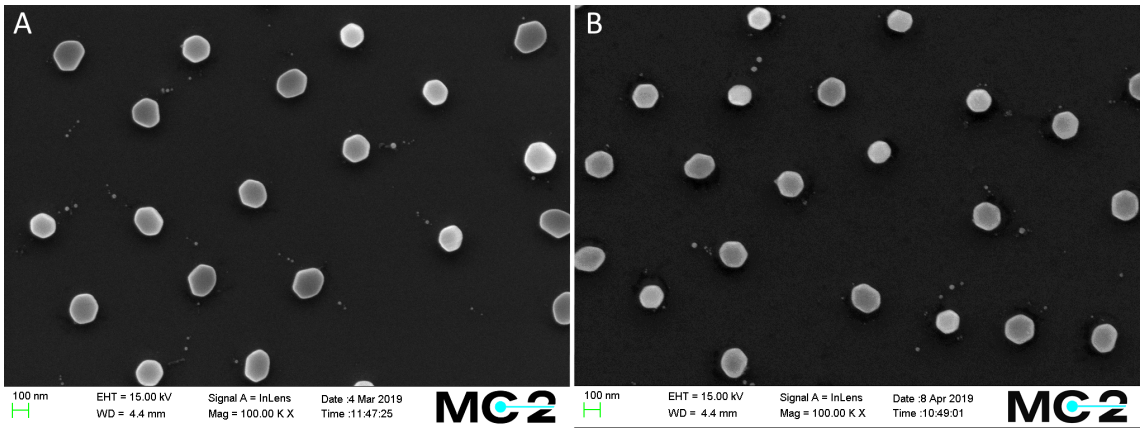

Figure 4.11: The results of doing the chemical process on Au particles whit A being before the process and B after.

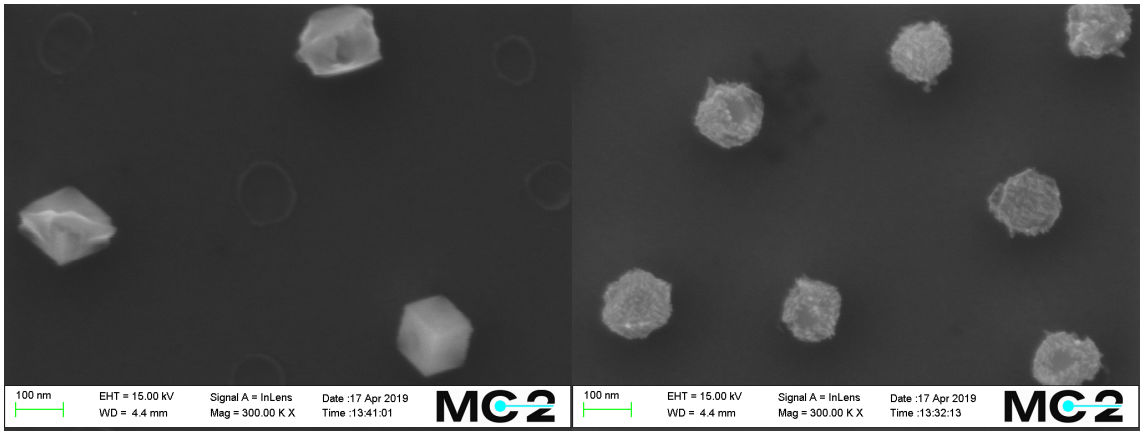

Figure 4.12: SEM images of Pd particles from HCl samples that were tested with the chemical process. The right image comes from particles that used the exact concentration of Pd salt as Preston et al. [6]. The particles in the left image were made using the same process but double the concentration

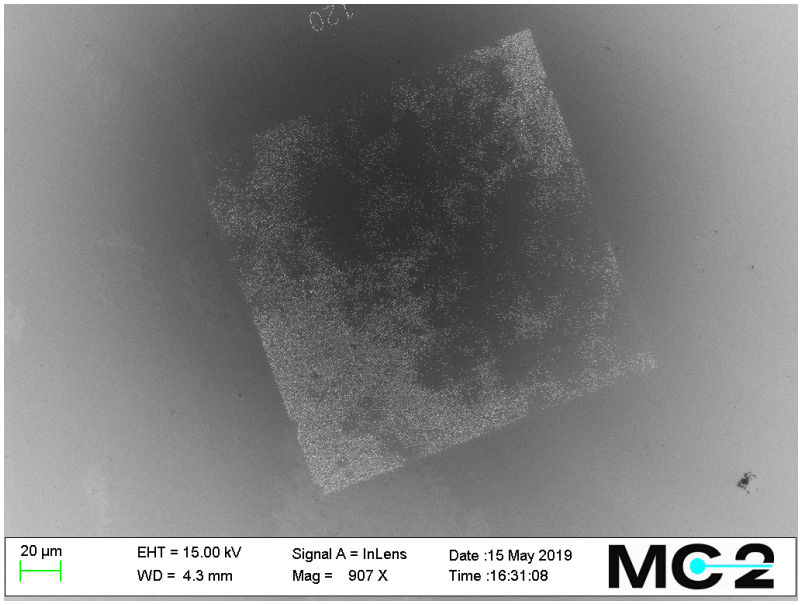

Figure 4.13: SEM Image of 120 nm Pd EBL fabricated samples that show the drop-off of particles from a square, that was originally a square array of nanoparticles, after the chemical process.

5
Discussion

5.1 Grains

Trying to fit the model from section 2.1.1 to the data acquired is not reasonable, instead, forming an alternative model based on the measured trends may be of more interest. Below is a relation that would be closer to the observed data than the bulk model.

$$g \propto \frac{D_p}{t}, e^{-\frac{aT}{T_m}} + 1 \tag{5.1}$$

This relation is fitted to experimental data of 250 nm particles and used to try predicting the temperature curve for 147 nm particles in figure 5.1. The expected curve for the 147 nm particles lays below the data points for 147 nm but with the large spread in the data this be considered close to the correct curve showing some predictive capabilities in this model.

Comparing the trends of the average number of grains detected in the results to the model based on bulk annealing in the theory section 2.1.1, one can see that the bulk-based model does not predict how the average number of grains should change over temperature or particle diameter. Comparing the fitted model in equation 5.1 to the Bulk model equation 2.5 is most interesting over temperature as it is the parameter most explored in this thesis. Furthermore, the shape of the bulk curve over temperature is not obvious from looking at the equation. The curves of the bulk and fitted model are plotted in figure 5.2 assuming a particle diameter of 200 nm with initially 100 grains and a 15 min annealing time. The constant A is approximated using the atomic volume ($V = 1.7 \cdot 10^{-2}$ nm^3), the grain width ($w = 1$ nm), the grain boundary surface energy ($Es = 0.5$ J/m^2) and an approximate experimental factor ($a = 5 \cdot 10^{-6}$) based on values from Lian e.tal [10].

$$A = \frac{4aVE_s}{w} \tag{5.2}$$

The classical value of the grain boundary migration activation energy (Q) for gold is 0.88 eV but the activation energy has shown to vary with the grain size and the strain of the annealed film [10, 32, 33, 34]. Choe e.tal showed that the activation energy for grain boundary migration more than doubled when the film was strained to a Q value of 1.95 eV [33]. Choe et al. explained this as a shift from grain boundary migration to lattice diffusion as the main factors of grain growth. Comparing both these values to the fitted model visualised in figure 5.2 one can see that these bulk curves lay on either side of the fitted model.

The bulk relation over temperature was based on the atomic mobility in grain boundaries, and difference in relation could indicate that grain mobility is not the main way of grain growth in the particles and other aspects play much larger roles in the grain growth of nanoparticles, especially as they dewet and approach single crystals. The fitted model could indicate an increase in Q value as the number of grains decrease and the grains

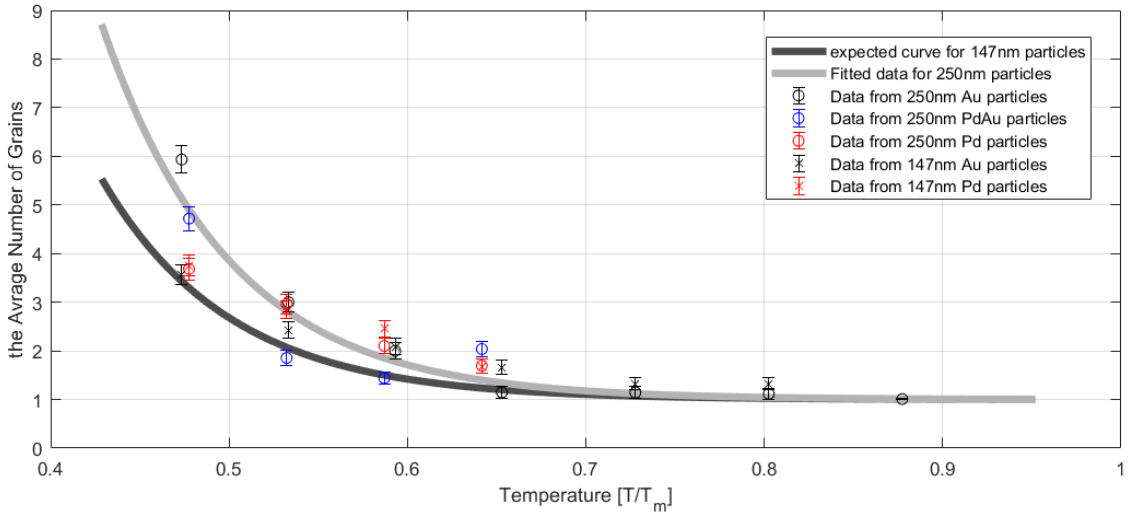

Figure 5.1: Here the model from equation 5.1 is fitted to the temperature data collected for 250 nm particles and using that fit the expected curve for 147 nm particles is calculated.

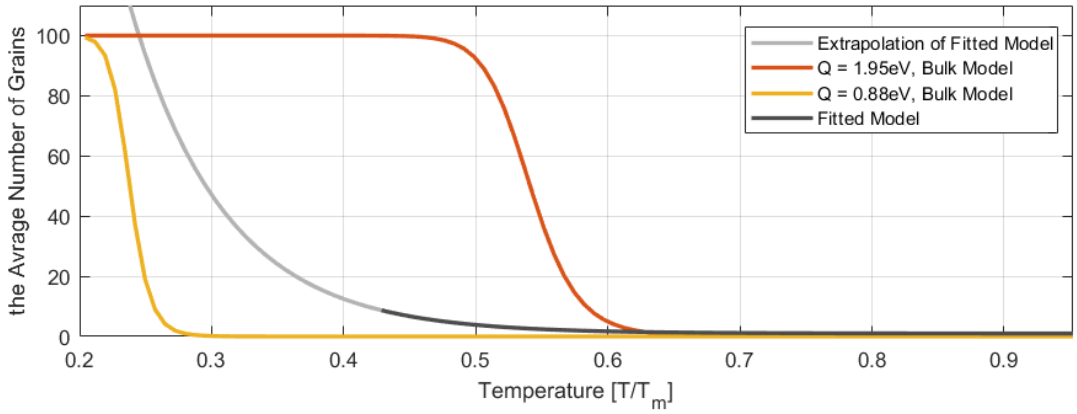

Figure 5.2: The bulk model of annealing compared to the fitted model found in this thesis compared for different Q values of the grain boundary migration.

become more constrained by the size of the particle, but further tests would need to be done to make any such conclusions.
The linear relation of the fabricated diameter to the average number of grains in the nanoparticles shows a slower increase in grains as the particles become bigger than expected. This difference could come from the straining of the grains by the size of the particle, potentially limiting the speed of grain growth more for smaller particles. No clear trend can be seen for the time in the measured data, but the evolution of grains is slow over time as expected from the bulk model.

5.1.1 The Parameters of Grains in a Particle

The data for how the average number of grains change with the size of fabricated discs clearly showed a linear relation in the range of sizes tested as seen in figure 4.7. It is also notable that the lines do not overlap, with exception to the very lower end of the bottom two lines, and that two lines with the same slope have very little offset from one another, even when they are produced using two different annealing methods and material. A linear trend with a specific slope does therefore appear to be linked to a specific size, where the particles reach single crystal, if they can reach single crystal.
This linear relation can however not hold true, as the grain structure approaches single crystal and the number of grains approach one. This is most clear for the steeper lines in figure 4.7, which would reach single crystal before the disk size reaches zero. In the near single crystal case, it would be expected that linear relation breaks down and a continuous, nonlinear, transition curve should form in the intersection to single crystallinity. This could be interesting to study by using a disk size and an annealing method that are known to produce single crystals and then increasing the disk size. This may however just cause the disk to separate into several single crystal particles like when dewetting a thin film [6, 12, 14, 15]. It is also worthy to note that the steeper lines, that come from process that produces a higher number of grains would reach single crystal before the shallower lines if the linear trend would be universally true. This gives rise to further questioning on how correct the linear relation is. Therefore, the linear trend should be considered as a local trend that most likely will not hold true for much larger changes in the size of fabricated disks than the ones used in these experiments.
The trend of grains over temperature does hold up a lot better to scrutiny than that over the diameter of fabricated disks. The number of grains decays exponentially towards one, when the temperature showing the evolution from polycrystalline nanoparticles to single crystal ones. The temperature needed to reach single crystal appears to be around 0.6 to 0.7 of the absolute melting temperature of the metal. This is the same relative temperature that structure zone diagrams indicate that films deposited at this temperature have a recrystallized grain structure with larger grains [31]. Tests on Y_2O_3 by Cantwell et al. have shown a large increase by an order of magnitude in the average size of grains when it was annealed over 0.63 - the relative absolute temperature compared to temperatures below that one [9]. An annealing temperature above 2/3 of the melting temperature does, from these examples, appear to trigger a large increase in the grain size and could potentially be used to form single crystal nanoparticles.

5.1.2 Detecting Grains with SEM

The method for measuring all the particles in this project have been SEM as it is an accessible and fast method of measurement of nanosize features, but there are some indications in the data collected how SEM is not optimal for measuring the grains in a particle. One of the clearest indications in how handling the SEM affected the data is in figure 4.7 when you compare all the data points of 150 nm fabricated particles and the 170 nm particles. Nearly all the points for the 150 nm are higher than the 170 nm of the same sample. This could be attributed to the difference in magnification in the SEM images taken for measuring the grain distributions of the two different sizes. All samples with discs larger than 150 nm were imaged using 100kx magnification, while those lower used 200kx magnification, when they were imaged for an overview of the number of grains. This was because more smaller particles could fit into the image with the same magnification and at 150 nm I felt I needed a closer look at the particles to see the grains. With higher magnification the grains became easier to see which likely led to the observation of grains that would not have been seen if the magnification had been 100kx. The difference in magnification can be seen in figure 5.3.

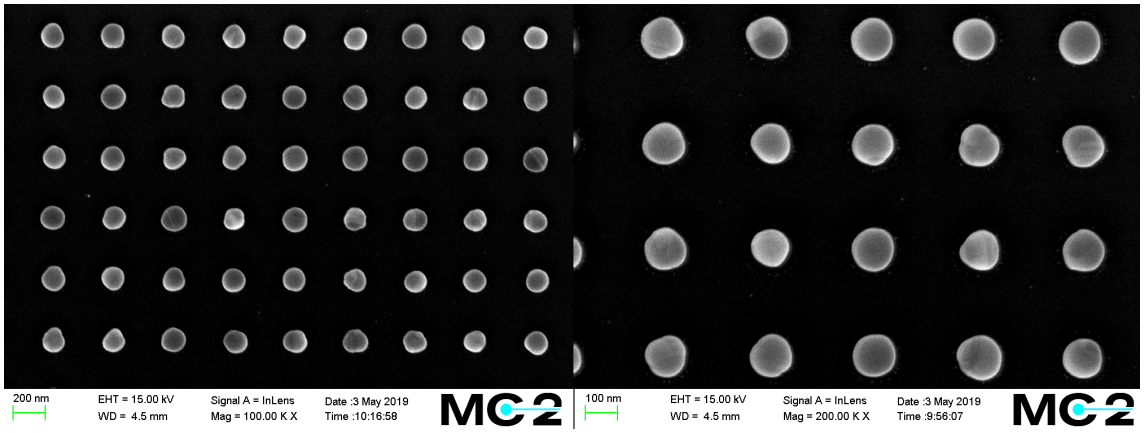

Figure 5.3: These are SEM images of EBL fabricated Au particles annealed at 440 °C for 15 min using RTP. The left image is of particles that had a diameter 170 nm before annealing, using 100kx magnification. The right image is of particles that had a diameter of 150 nm before annealing, using 200kx magnification.

The example of difference between 100kx and 200kx magnification does not only apply to the example shown, but to all the measurements that have been done. Many smaller grains can therefore have been missed, when the grain measurements were taken resulting in larger errors when measuring small particles and particles with many grains. This error should however be smaller when you look at the measurement of larger near single crystal particles which generally have more clearly defined grains.
Another problem whit the imagining was that grains of Cu particles were hard to image as small amounts of oxygen gets into the annealing process causing oxidation on the surface of the Cu. In the best case, only a light blurring tint could be seen on the particles, but larger formation that obscures the particle beneath could also form on the surface. The usage of shorter annealing times at higher temperatures worked well to minimise the oxidation but it could not be prevented. An example of how Cu particles look when they are completely covered in oxide can be seen in figure 5.4. Because of this oxide it was particularly hard to detect the grains of the Cu particles, which is why measurements of these particles are missing from all the graphs tracking the number of

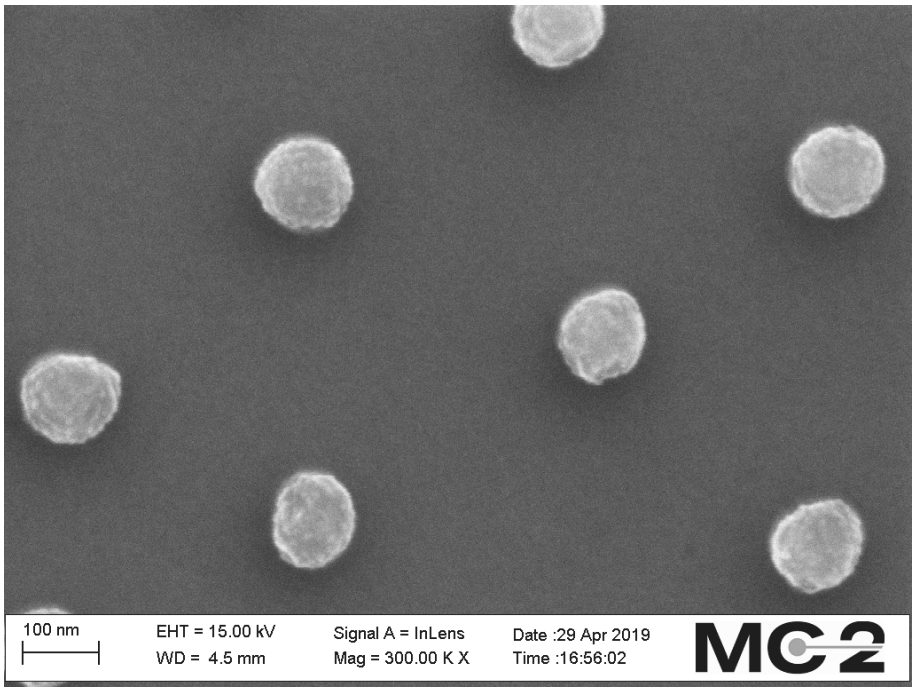

Figure 5.4: This SEM image shows a sample of Cu particles that where first annealed at 900 °C for 1 min and then annealed at 24 h at 500 °C. This was an attempt to first dewet the structure and then let the grains grow to single crystals. However, the only clear result is the formation of a thick oxide.

grains over different parameters. The grains of oxidised Cu particles can be measured using transmission electron microscopy (TEM), which is overall a better way to measure the amount of grains of a particle compared to SEM especially if one uses Transmission Kikuchi diffraction (TKD) which is a mode of TEM particularly good at detecting crystal grains [35].

5.1.3 The Types of Grains in a Nanoparticle

In all the data taken in this project, all grain boundaries have been considered equal, while there are notable differences in how different types of grain boundaries affect the properties of the nanoparticle and how the different grain boundaries behave under the effects of annealing. The grain boundaries of metal nanoparticles can be characterised in two categories: High angle grain boundaries and twin boundaries, low angle grain boundaries are uncommon in the grain structure of nanoparticles and can therefore be neglected [4]. In experiments where gold films were dewetted to produce single crystal particles, they found that the most common defect in the non-single crystal particles were twin boundaries [14]. A brief overview of my near single crystal particle samples seems to show similar trend, but no distribution has been taken, as the difference between the types of grain boundaries is hard to detect in SEM images. It would be reasonable to expect that the grain boundaries of the near single crystal would more likely be twin boundaries as it has a lower defect energy compared to high angle grain boundaries.

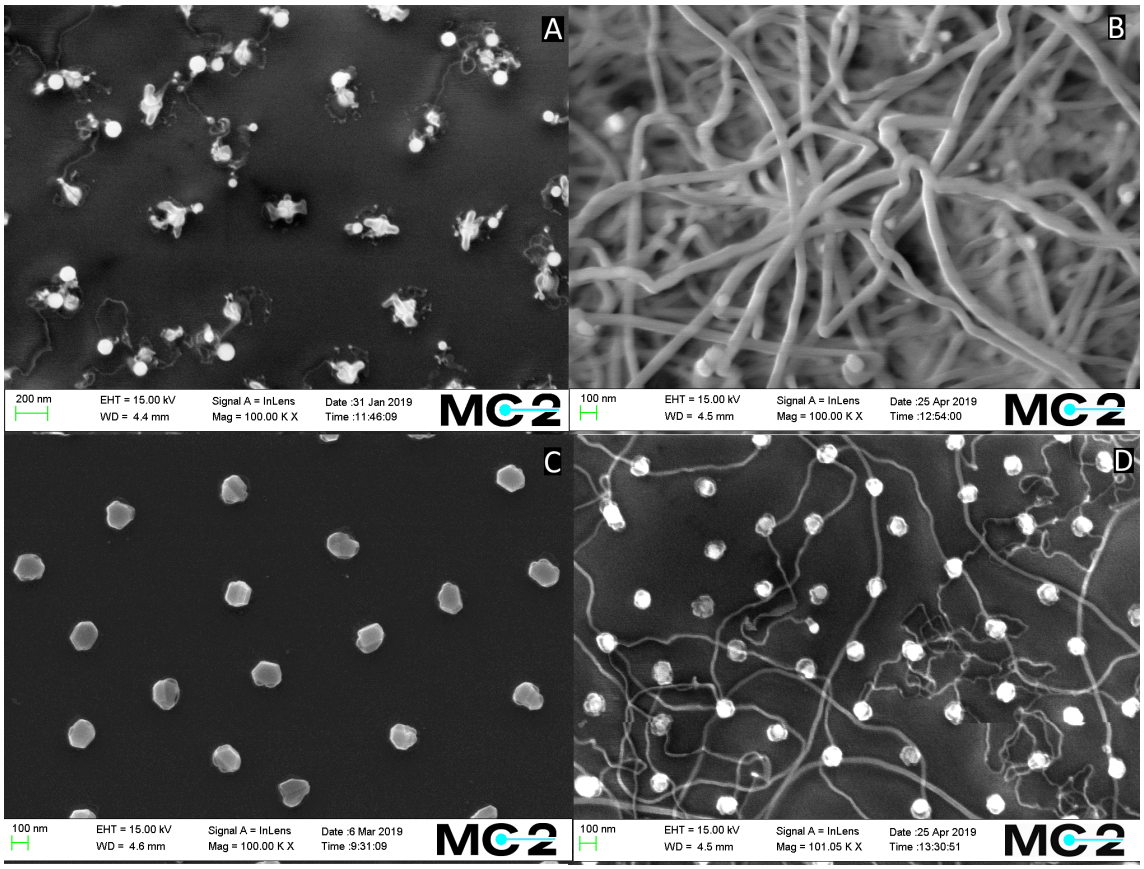

Figure 5.5: Images of Pd particles annealed in the Thermolyne furnace. A and B where annealed at 1085 °C where A used a thicker substrate oxide and was left to cool upon reaching the temperature and B used a thinner substrate oxide and was held for one hour. C and D where annealed at 960 °C for 2 h, where C had a thicker substrate oxide and D used a thinner substrate oxide.

5.1.4 Making Single Crystal Pd Particles

In the attempts to control the grain distributions of the number of grains it was shown that an increase in temperature is the most effective way of producing single crystal nanoparticles. This was however seen primarily using Au particles as Pd particles require a higher temperature to create single crystals than the max temperature allowed to be used in the RTP. The temperature that has appeared to be necessary to create a sample with most single crystal particles is above 0.7 of the absolute temperature as discussed earlier in section 5.1.1 and for Pd this would mean a temperature above 1008 °C. The only reactor available that can create this high of a temperature is the Thermolyne reactor, but in the tests in which this reactor was used it was common to see contaminations or strange formations on the sample. Examples of how these samples look like can be seen in figure 5.5.
In the literature one can find more novel approaches to make single crystal dewetted Pd particles when straight forward annealing is not enough. Preston et al. needed to use a sacrificial layer of Bi to create dewetted Pd particles but still used a temperature of 1100 °C, which is well over the temperature that is expected to be needed to create single crystal particles [6]. This could have been necessary because of the use of a sapphire substrate, which most likely affect the dewetting characteristics of the particles. Sundar

et al. created faceted Pd particles by annealing a set of single crystal Au particles, as a sacrificial template, in contact with a Pd foil [36]. This used an annealing temperature of 1080 °C and causing a net migration of Pd to the sample and the Au particles to be replaced with faceted Pd particles. From these examples one could conclude that the 1008 °C temperature suggested above, to create single crystal Pd particles may not be enough and that a basic annealing process might require even higher temperature to create single crystal Pd particles.

5.2 Shape

When comparing the EBL fabricated particles with those fabricated by HCL, the EBL produced particles were rounder and more uniform in shape. There are two things that I can see as major factors in how the two fabrication methods differ in this aspect: fabrication defects and a difference in adhesion because of different treatments of the substrate.
The difference in fabrication defects can be seen when comparing the fabricated disks that were used for the annealing experiments and a comparison can be seen in figure 5.6. The disks fabricated using HCL have rougher edges compared to the EBL produced particles and HCL disks also have spikes and satellites that could cause the edge defects seen in the annealed HCL samples.

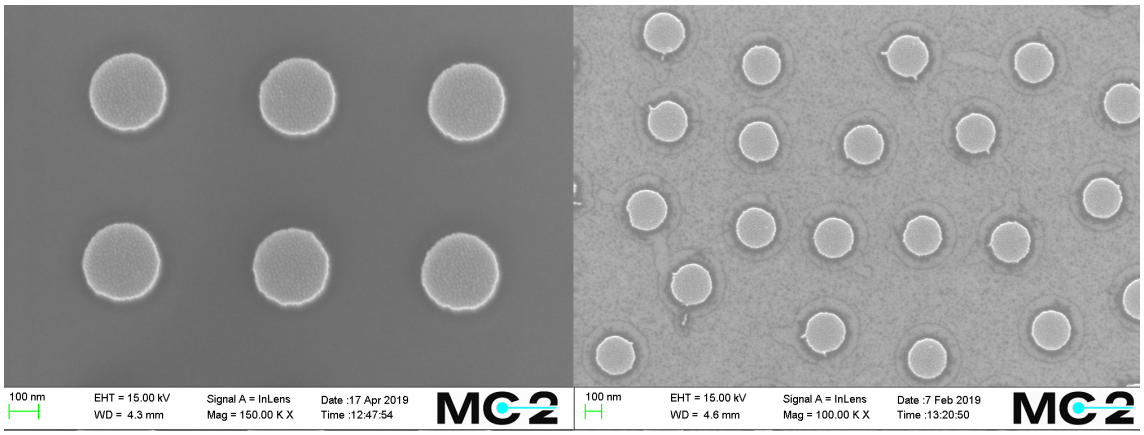

Figure 5.6: These SEM images are of Pd with 10% Au disks with a diameter of about 250 nm. The left is an image of EBL fabricated disks at a magnification of 150kx and the right image is of HCL fabricated disks at a magnification of 100kx.

The potential difference in adhesion between HCL and EBL could cause the EBL samples to more easily dewet and form rounder uniform particles as suggested in section 2.1.2 of the theory. From the results of trying to chemically facet the EBL samples we can see that they were much more prone to fall off the substrate compared to the HCL fabricated samples indicating a weaker adhesion. Therefore, one can suspect that the EBL samples have weaker adhesion to the substrate and that this contributes to the rounder particles from EBL fabricated disks. This may be caused by the building of charges in the surface after exposure in the EBL process as this would change the functionality of the substrate surface, potentially altering how the metals interact with the substrate. It would be interesting to try, if one can Improve the adhesion of EBL samples without losing “roundness” of the particles as having both are important for the chemical faceting of the nanoparticles.

5.2.1 Faceting

When attempting to facet the particles, most particles turned out in odd non-symmetric shapes. This clearly shows that the chemical process needs to be tuned to get a good control of the facets of the particle. However, there where symmetric faceted particles among the particles that went through the chemical process, showing potential for the process used to be able to control the faceting and surfaces of nanoparticles. With a few more tests it should be possible to recreate the faceted Wulff-shaped particles produced by Preston et al. [6]

The Pd particles formed cubes in the chemical growth process indicating that the process favoured the {100} facet as the surface structure. Pd cubes that where of a similar size, with {100} faces, have been synthesised by Niu et al., using the same chemicals used in this project (H_2PdCl_4, CTAB and AA), from 22 nm Pd cubes [37]. Niu et al. were also able to create particles with only {110} and {111} facets from the same seeds by varying the temperature and adding different concentrations of potassium iodide (KI). This opens an opportunity that this could also be done to the single crystal particles fabricated using an annealing process to control the surface structure of ordered nanoparticles. This is further interesting as the facet of the metal has shown in simulations to play a large role in effectiveness of catalysis and its control can improve the catalytic capabilities of Pd nanoparticles [5].

The Cu and Au particles both formed more Wulff-shaped structures as was originally intended with the recipe, with the difference that the Cu particles grew a lot more than the Au particles. The poor growth of the Au particles is suspected to have been caused by the flat-topped particles that likely adsorbed a lot of the material as they are large surface, which require a lot of material to grow to an equilibrium shape. The recipe for the Cu particles did not include a dedicated surfactant, which could control and inhibit the growth. To get a better control of Cu it would be interesting to check the concentration of Cu-salt used and check for a surfactant that may be used to control the face of the surface. For Au particles, a clearer change can hopefully be seen from a more dewetted structure and a higher concentration of Au salts.

6
Conclusion

6.1 Controlling the Grain Structure of Nanoparticles with Annealing

The number of grains in nanoparticles could successfully be controlled by altering the temperature of annealing and the diameter of the fabricated metal disk. The average number of grains over temperature showed an exponential decay towards single crystal with a tendency to reach single crystal at a temperature near 0.7 of the absolute melting temperatures of the metal for both gold and palladium. The approximate equation that describes the average number of grains in 250nm diameter gold or palladium nanoparticles as function of annealing temperature can be seen below.

$$\left(1 + e^{8.0 - 13.9\frac{T}{T_m}}\right)$$

The average number of grains over the diameter of the particle showed a rising linear relationship for particles in the size range of 100 nm to 270 nm with a slope depending on material, temperature and time. This relation is not expected to hold for a large expansion of the range, but it can be used to control the number of grains for particles within the range. Time also plays a large role but longer times then those tested in this project are necessary to see a clear trends other than fewer grains with longer annealing time.
The annealing also changed the shape of the particles corelated with the number of grains in the particle. Particles with many grains (over 5) generally showed a flat circular disk structure and as the number of grains reduced the particle takes on more odd shapes. This continues until the particles approach the single crystal limit and form round dewetted structures.

6.2 Controlling the Faces of Nanoparticles

In these tests it has been shown that the chemical method of colloidal synthesis can be applied to top down fabricated metal nanoparticles in order to control the shape and faces of the metal nanoparticle. While an optimal recipe has not been discovered yet, the process shows an easy way to modify the nanoparticles that would be very hard to make using top down processes. This while retaining the control of the particles position on a substrate which is easily controlled using top down methods. Further tests need to be done to achieve control over what faces will appear on the particle.

Bibliography

[1] F. A. A. Nugroho, I. Darmadi, L. Cusinato, A. Susarrey-Arce, H. Schreuders, L. J. Bannenberg, A. B. da Silva Fanta, S. Kadkhodazadeh, J. B. Wagner, T. J. Antosiewicz, A. Hellman, V. P. Zhdanov, B. Dam, and C. Langhammer, "Metal–polymer hybrid nanomaterials for plasmonic ultrafast hydrogen detection," *Nat. Mater.*, vol. 18, pp. 489–495, may 2019.

[2] C. Wadell, F. A. A. Nugroho, E. Lidström, B. Iandolo, J. B. Wagner, and C. Langhammer, "Hysteresis-free nanoplasmonic pd-au alloy hydrogen sensors," *Nano Lett.*, vol. 15, no. 5, pp. 3563–3570, 2015.

[3] F. A. A. Nugroho, I. Darmadi, V. P. Zhdanov, and C. Langhammer, "Universal Scaling and Design Rules of Hydrogen-Induced Optical Properties in Pd and Pd-Alloy Nanoparticles," 2018.

[4] S. Alekseeva, A. B. D. S. Fanta, B. Iandolo, T. J. Antosiewicz, F. A. A. Nugroho, J. B. Wagner, A. Burrows, V. P. Zhdanov, and C. Langhammer, "Grain boundary mediated hydriding phase transformations in individual polycrystalline metal nanoparticles," *Nat. Commun.*, vol. 8, no. 1, 2017.

[5] B. Hagman, A. Posada-Borbón, A. Schaefer, M. Shipilin, C. Zhang, L. R. Merte, A. Hellman, E. Lundgren, H. Grönbeck, and J. Gustafson, "Steps Control the Dissociation of CO2 on Cu(100)," *J. Am. Chem. Soc.*, vol. 140, pp. 12974–12979, oct 2018.

[6] A. S. Preston, R. A. Hughes, T. B. Demille, V. M. Rey Davila, and S. Neretina, "Dewetted nanostructures of gold, silver, copper, and palladium with enhanced faceting," *Acta Mater.*, vol. 165, pp. 15–25, 2019.

[7] F. Humphreys and M. Hatherly, *Recrtstallization and Related Annealing Pheneomena*. Elsevier, 2002.

[8] G. Totten, *ASM Handbook*. 2018.

[9] P. R. Cantwell, S. Ma, S. A. Bojarski, G. S. Rohrer, and M. P. Harmer, "Expanding time–temperature-transformation (TTT) diagrams to interfaces: A new approach for grain boundary engineering," *Acta Mater.*, vol. 106, pp. 78–86, mar 2016.

[10] J. Lian, R. Z. Valiev, and B. Baudelet, "On the enhanced grain growth in ultrafine grained metals," *Acta Metall. Mater.*, vol. 43, pp. 4165–4170, nov 1995.

[11] J. P. Enríquez and X. Mathew, "XRD study of the grain growth in CdTe films annealed at different temperatures," in *Sol. Energy Mater. Sol. Cells*, vol. 81, pp. 363–369, feb 2004.

[12] F. Ruffino and M. G. Grimaldi, "Self-organized patterned arrays of Au and Ag nanoparticles by thickness-dependent dewetting of template-confined films," *J. Mater. Sci.*, vol. 49, no. 16, pp. 5714–5729, 2014.

[13] P. Pandey, S. Kunwar, M. Sui, S. Bastola, and J. Lee, "Role of annealing temperature, time, and composition on the fabrication of AUxPd1-x nanostructures on c-plane sap-

phire by the solid-state dewetting of bimetallic thin films," *IEEE Trans. Nanotechnol.*, vol. 17, no. 2, pp. 325–331, 2018.
[14] H. Sadan and W. D. Kaplan, "Au-Sapphire (0001) solid-solid interfacial energy," in *J. Mater. Sci.*, vol. 41, pp. 5099–5107, 2006.
[15] F. Leroy, Borowik, F. Cheynis, Y. Almadori, S. Curiotto, M. Trautmann, J. C. Barbé, and P. Müller, "How to control solid state dewetting: A short review," 2016.
[16] D. Chatain, V. Ghetta, and P. Wynblatt, "Equilibrium Shape of Copper Crystals Grown on Sapphire," *Interface Sci.*, vol. 12, no. 1, pp. 7–18, 2004.
[17] C. M. Müller, F. C. F. Mornaghini, and R. Spolenak, "Ordered arrays of faceted gold nanoparticles obtained by dewetting and nanosphere lithography," *Nanotechnology*, vol. 19, no. 48, 2008.
[18] E. Ricci and R. Novakovic, "Wetting and surface tension measurements on gold alloys," *Gold Bull.*, vol. 34, no. 2, pp. 41–49, 2001.
[19] F. Ruffino and M. G. Grimaldi, "Roughness evolution in dewetted Ag and Pt nanoscale films," *Superlattices Microstruct.*, vol. 113, pp. 430–441, 2018.
[20] W. Winterbottom, "Equilibrium shape of a small particle in contact with a foreign substrate," *Acta Metall.*, vol. 15, pp. 303–310, feb 1967.
[21] D. M. Lipkin, D. R. Clarke, and A. G. Evans, "Effect of interfacial carbon on adhesion and toughness of gold-sapphire interfaces," *Acta Mater.*, vol. 46, pp. 4835–4850, aug 1998.
[22] L. Reimer, *Scanning Electron Microscopy*, vol. 171. 1985.
[23] B. J. Griffin, "A comparison of conventional Everhart-Thornley style and in-lens secondary electron detectors-a further variable in scanning electron microscopy," *Scanning*, vol. 33, no. 3, pp. 162–173, 2011.
[24] M. Faraday, "The Bakerian Lecture : Experimental Relations of Gold (and Other Metals) to Light Author (s): Michael Faraday Source : Philosophical Transactions of the Royal Society of London , Vol . 147 , No . (1857), pp . 145-181 Published by : The Royal Society," *Philos. Trans. R. Soc. London*, vol. 147, pp. 145–181, jan 1857.
[25] Cademartiri. L and Ozin. G.A, "Concept of Nanochemistry," Weinheim: WILEY-VCH Verlag GmbH & Co, 2009.
[26] Y. Xia, K. D. Gilroy, H.-C. Peng, and X. Xia, "Seed-Mediated Growth of Colloidal Metal Nanocrystals," *Angew. Chemie*, vol. 129, no. 1, pp. 60–98, 2017.
[27] T. K. Sau and A. L. Rogach, *Complex-shaped Metal Nanoparticles.* Weinheim: WILEY-VCH, 2012.
[28] H. Fredriksson, Y. Alaverdyan, A. Dmitriev, C. Langhammer, D. S. Sutherland, M. Zäch, and B. Kasemo, "Hole-mask colloidal lithography," *Adv. Mater.*, vol. 19, no. 23, pp. 4297–4302, 2007.
[29] A.-P. Blanchard-Dionne and M. Meunier, "Electron beam lithography using a PMMA/P(MMA 8.5 MAA) bilayer for negative tone lift-off process," *J. Vac. Sci. Technol. B, Nanotechnol. Microelectron. Mater. Process. Meas. Phenom.*, vol. 33, no. 6, p. 061602, 2015.
[30] "ImageJ," *https://imagej.nih.gov/ij/*, 2019-06-12.
[31] A. Anders, "A structure zone diagram including plasma-based deposition and ion etching," *Thin Solid Films*, vol. 518, no. 15, pp. 4087–4090, 2010.
[32] G. Guisbiers and L. Buchaillot, "Size and shape effects on creep and diffusion at the nanoscale," *Nanotechnology*, vol. 19, oct 2008.
[33] J. W. Choe, J. N. Calata, and G. Q. Lu, "Constrained-film sintering of a gold circuit paste," *J. Mater. Res.*, vol. 10, no. 4, pp. 986–994, 1995.

[34] A. Gangulee and F. M. D'Heurle, "The activation energy for electromigration and grain-boundary self-diffusion in gold," *Scr. Metall.*, vol. 7, no. 10, pp. 1027–1030, 1973.

[35] G. C. Sneddon, P. W. Trimby, and J. M. Cairney, "Transmission Kikuchi diffraction in a scanning electron microscope: A review," *Mater. Sci. Eng. R Reports*, vol. 110, pp. 1–12, dec 2016.

[36] A. Sundar, P. Farzinpour, K. D. Gilroy, T. Tan, R. A. Hughes, and S. Neretina, "Organized surfaces of highly faceted single-crystal palladium structures seeded by sacrificial templates," *Cryst. Growth Des.*, vol. 13, no. 9, pp. 3847–3851, 2013.

[37] W. Niu, L. Zhang, and G. Xu, "Shape-controlled synthesis of single-crystalline palladium nanocrystals," *ACS Nano*, vol. 4, no. 4, pp. 1987–1996, 2010.

A

Appendix

A.1 Matlab code for getting grain distributions

```
choice='Filename';

toData='~/path_to_file_folder;
grainFs=['00';'01';'02';'03'];
a='';
for i=1:4
    a=char(a, strcat(toData,choice,grainFs(i,:),'.txt'));
end
b=char(ones(4,size(a,2)) * 'a');
for i=2:5
    b(i-1,:)= a(i,:);
end
grainSet=b;
%% setting
% chose data from above
arrayData=grainSet; % list datasets frome above%% settings

min=0;
max=14; % must be larger than the largest particle
pW=1; % width of bars
figWidth=3; % 2.85-half page 6-whole page
figHight=1.8;

%figure
colormap lines; %lines %hot
xlab='Grains per Particle';
ylab='Normalised Particle Count';
barON=1; % if 1 plot bars
poiON=1; % if 1 plot normal distribution
cOff=1; % colour offset of norm to bar
barWidth=1;
%% if build
toData='C:/Users/jberg/OneDrive/exJobb/SEM_data';
l2=size(toData);
l2=l2(2);
n=size(arrayData);
l=n(2)+l2;
n=n(1);
arrayData2 = char(ones(n,l) * 'a');
strcat(arrayData(1,:));
for i=1:n
    a=char(strcat(arrayData(i,:)),arrayData2(1,:));
    arrayData2(i,:)=a(1,:);
end

%%
span = max-min;
clf
%figure
hold on
data=load(arrayData2(1,:));
A=data(:,[2,6,7]);
i=1;
while A(i,1)>0
    i=i+1;
end

Gpp=zeros(1,span);
Ys=zeros(n,i-1);
Ns=zeros(n,i-1);
setSize=zeros(1,n);

setSize(1)=size(A,1);
    [N,Y,~]=getGD(A);
```

```
    Ys(1,:)=Y;
    Ns(1,:)=N;
if n>1
    for i=1:n
        data=load(arrayData2(i,:));
        iii=1;
        A=data(:,[2,6,7]);
        setSize(i)=size(A,1);
        [N,Y,~]=getGD(A);
        Y;
        for j=1:size(Y,2)
            Gpp(Y(j))=Gpp(Y(j))+1;
        end
        %plot(X,N,'linewidth',2); %,'color','red'
    end
end
X=linspace(1,span,span);
num=0;
tot=0;
for i=1:span
    num=num+Gpp(i);
    tot=tot+i*Gpp(i);
end
mean=tot/num
er=sqrt(mean/num)
poi = poisspdf(X-ones(1,span),mean-1);
Gpp=Gpp/num;


if barON == 1
    bars=bar(X,Gpp,barWidth);

    cm = colormap;
end

hold on
if poiON == 1
    pn = plot(X,poi,'--','linewidth',2,'color','r');
end


xlim([min max])
xlabel(xlab);
ylabel(ylab);
grid on
latex_fig( 12, figWidth, figHight);
-------------------------------------------
function [y,N,x] = getGD(A)

i=1;
while A(i,1)>0
    i=i+1;
end
ps=A(1:i-1,:);
gs=A(i:end,:);

Sps=ps;
Sgs=gs;

p=i;
gpp=zeros(1,p-1);
x=linspace(1,p-1,p-1);
for j=1:p-1
    px=Sps(j,2);
```

```
    py=Sps(j,3);
    pr=2*sqrt(Sps(j,1)/pi);

    k=1;
    while py-2*pr > Sgs(k,3)
        k=k+1;
    end
    legnth=size(Sgs,1);
    while py+2*pr > Sgs(k,3)
        if (Sgs(k,3)-py)^2+(Sgs(k,2)-px)^2 < pr^2
            gpp(j)=gpp(j)+1;
        end
        k=k+1;
        if k == legnth+1
           break
        end

    end
end

y=gpp;
N=gpp;
end
```